Copy
RM L56L28

NACA RM L56L28

C.1

NACA

RESEARCH MEMORANDUM

DYNAMIC STABILITY INVESTIGATION OF TWO RIGHT CIRCULAR CYLINDERS IN AXIAL FREE FLIGHT AT MACH NUMBERS FROM 0.4 TO 1.7

FINENESS-RATIO-2.56 CYLINDER AND FINENESS-RATIO-4.0 CYLINDER WITH FLARED AFTERBODY

By John C. McFall, Jr.

Langley Aeronautical Laboratory
Langley Field, Va.

NATIONAL ADVISORY COMMITTEE
FOR AERONAUTICS

WASHINGTON

February 28, 1957

[redacted]

NATIONAL ADVISORY COMMITTEE FOR AERONAUTICS

RESEARCH MEMORANDUM

DYNAMIC STABILITY INVESTIGATION OF TWO RIGHT CIRCULAR CYLINDERS IN AXIAL FREE FLIGHT AT MACH NUMBERS FROM 0.4 TO 1.7

FINENESS-RATIO-2.56 CYLINDER AND FINENESS-RATIO-4.0 CYLINDER WITH FLARED AFTERBODY

By John C. McFall, Jr.

SUMMARY

Two right circular cylinders have been tested in axial free flight over a Mach number range of 0.4 to 1.7 and a Reynolds number range of 1×10^6 to 8×10^6 by using the rocket-boosted-model technique. When given a large disturbance at supersonic speeds, both the fineness-ratio-2.56 cylinder and the fineness-ratio-4.0 cylinder with flared afterbody damped from a large-amplitude coupled motion at supersonic speeds to a low-amplitude sustained oscillation at low subsonic speeds. The variation of moment coefficient with force coefficient was nonlinear, the region of most stable slope occurring at the zero force coefficient. For both cylinders the average center of pressure over the force-coefficient range of ± 0.5 moved rearward with decrease in speed to subsonic Mach numbers. Although large pitching and yawing motions were observed, there were no large deviations from a ballistic trajectory. Comparison of the drag data of this test with the drag data from the wind-tunnel and free-flight helium-gun tests indicates that the friction drag is a very small part of the total drag. The presence of the afterbody flare on the fineness-ratio-4.0 cylinder causes an increase of about 20 percent of the total drag over the drag of a cylinder with no flare at low supersonic speeds.

INTRODUCTION

The unusual requirements of very low lift and very high drag for aerodynamic shapes have become of general interest in the design of

[redacted]

various stores. (See refs. 1 and 2.) One configuration which meets these unusual requirements is a right circular cylinder in axial flow. An investigation is being conducted by the Langley Pilotless Aircraft Research Division with the rocket-boosted free-flight-model technique to determine the dynamic stability of right circular cylinders in axial free flight. This paper presents the results from flight tests of a right circular cylinder having a fineness ratio of 2.56 and a right circular cylinder with a flared afterbody and having a fineness ratio of 4.0. These tests covered a Mach number range from 0.4 to 1.7 and a Reynolds number range from 1×10^6 to 8×10^6 based on the cylinder diameter. The free-flight tests were conducted at the Langley Pilotless Aircraft Research Station at Wallops Island, Va.

SYMBOLS

$a_{n,1}$ normal accelerometer reading from accelerometer in forward end of cylinder, g units

$a_{n,2}$ normal accelerometer reading from accelerometer in rear end of cylinder, g units

$a_{t,1}$ transverse accelerometer reading from accelerometer in forward end of cylinder, g units

$a_{t,2}$ transverse accelerometer reading from accelerometer in rear end of cylinder, g units

x distance along cylinder from nose, ft

$x_{n,1}$ displacement of $a_{n,1}$ accelerometer from center of gravity, positive forward, ft

$x_{n,2}$ displacement of $a_{n,2}$ accelerometer from center of gravity, positive forward, ft

$x_{t,1}$ displacement of $a_{t,1}$ accelerometer from center of gravity, positive forward, ft

$x_{t,2}$ displacement of $a_{t,2}$ accelerometer from center of gravity, positive forward, ft

$\ddot{\theta} - \dot{\psi}\dot{\phi}$ pitching acceleration, $g\frac{a_{n,2} - a_{n,1}}{x_{n,2} - x_{n,1}}$, radians/sec^2

[redacted]

$a_{n,cg}$ normal acceleration, $\frac{a_{n,1}x_{n,2} - a_{n,2}x_{n,1}}{x_{n,2} - x_{n,1}}$, g units

$\ddot{\psi} + \dot{\theta}\dot{\phi}$ yawing acceleration, $g\frac{a_{t,2} - a_{t,1}}{x_{t,2} - x_{t,1}}$, radians/sec^2

$a_{t,cg}$ transverse acceleration, $\frac{a_{t,1}x_{t,2} - a_{t,2}x_{t,1}}{x_{t,2} - x_{t,1}}$, g units

$a_{l,cg}$ longitudinal accelerometer reading, g units

C_N normal-force coefficient, $a_{n,cg}\frac{W}{S/q}$

C_Y lateral-force coefficient, $a_{t,cg}\frac{W}{S/q}$

C_R resultant-force coefficient, $\sqrt{C_N^2 + C_Y^2}$

C_D drag coefficient based on cross-sectional area

C_C longitudinal-force coefficient, $a_{l,cg}\frac{W}{S/q}$

C_n yawing-moment coefficient, $\frac{I_Z}{qSd}\left(\ddot{\psi} + \dot{\theta}\dot{\phi}\right)$

C_m pitching-moment coefficient, $\frac{I_Y}{qSd}\left(\ddot{\theta} - \dot{\psi}\dot{\phi}\right)$

x_{cg} center of gravity

d diameter of cylinder, ft

g acceleration due to gravity, ft/sec^2

I_X, I_Y, I_Z moments of inertia, slug-ft^2

l length of cylinder, ft

M Mach number

[redacted]

q	dynamic pressure, lb/sq ft
R	Reynolds number based on cylinder diameter
S	cross-sectional area of cylinder, sq ft
W	weight of cylinder, lb
α	angle of attack, radians
θ	angle of pitch, radians
ϕ	angle of roll, radians
ψ	angle of yaw, radians

A dot above a symbol indicates time rate of change of symbol; for example, $\dot{\theta} = \frac{\partial \theta}{\partial t}$.

The time sequence for the cross plots is indicated by the symbols ○, □, ◇, ◁, △, and ▱; the symbols change at each maximum and each minimum value of C_Y.

CYLINDERS

The physical characteristics of the cylinders are presented in figures 1 and 2 and table I.

The fineness-ratio-2.56 cylinder was a right circular cylinder with a diameter of 8 inches. The center of gravity was located at 32.3 percent of the cylinder length behind the nose. The fineness-ratio-4.0 cylinder was a right circular cylinder with a diameter of 8 inches and had a 13° flare that began 4.84 inches from the rear end of the cylinder and ended 1.25 inches from the rear end of the cylinder. The remainder of the afterbody consisted of a circular cylinder section with a diameter of 9.66 inches. The center of gravity of the fineness-ratio-4.0 cylinder was located at 25 percent of the body length from the nose.

The cylinders were constructed of welded steel and were covered with a fiberglass-plastic shell. Two small rockets (called pulse rockets) were mounted normal to the longitudinal axis and ahead of the center of gravity to give a yaw disturbance.

INSTRUMENTATION

Each cylinder contained an NACA six-channel telemeter which transmitted data from six accelerometers located as follows: one normal and one transverse accelerometer in the forward end of the cylinder; two longitudinal accelerometers near the center of gravity; and one normal and one transverse accelerometer in the rear end of the cylinder. A measure of the signal strength transmitted from the loop antenna provided an indication of the roll rate of the cylinders since the strength of the signal varied with the cylinder roll position.

Ground instrumentation included a CW Doppler radar unit used for velocity measurement, an SCR 584 tracking radar to determine the flight path, a rawinsonde to determine the atmospheric conditions, and the telemeter receiving and recording stations. Motion-picture cameras were used to photograph the launching and cylinder-booster separation portions of the flight.

FLIGHT TESTS

The cylinders were ground launched at an angle of 70° from the horizontal by an ABL Deacon solid-propellant rocket motor booster. Separation of the cylinder from the spent booster was accomplished by the opening of the drag flaps attached to the booster. Motion pictures of the cylinder-booster separation indicated that the cylinders oscillated to angles of at least $\pm 30^{\circ}$ immediately after leaving the booster. This large disturbance was caused partly by the booster pulling away and partly by the firing of one of the pulse rockets as soon as the cylinder cleared the booster. Tracking radar showed that the cylinders followed an approximately parabolic flight path with no change in azimuth.

ACCURACY

For the fineness-ratio-2.56 cylinder some indication of instrumentation malfunctions (instantaneous changes in absolute values of the measured quantities) make it impossible to state any absolute accuracy. However, since the data for the fineness-ratio-2.56 cylinder were corrected for the observed malfunctions and none were observed for the data for the fineness-ratio-4.0 cylinder, some indication of accuracy is obtained from the instrument accuracies which are estimated to be ±2 percent of the full calibrated range. The incremental values and relative

trends are much more accurate than the absolute level of the measurements. The instrument accuracies are stated in coefficient form for representative Mach numbers as follows:

Coefficient	Fineness-ratio-2.56 model at Mach numbers of -			Fineness-ratio-4.0 model at Mach numbers of -		
	1.4	0.8	0.4	1.4	0.8	0.4
C_N	±0.022	±0.071	±0.31	±0.024	±0.078	±0.340
C_Y	±.022	±.071	±.31	±.024	±.078	±.340
C_C	±.025	±.081	±.36	±.018	±.059	±.256

PRESENTATION OF RESULTS

The positive directions of the force and moment coefficients and angular velocities are indicated in figure 3. The Reynolds number range of the cylinder flights are shown in figure 4 and the flight paths are given as plots of altitude against horizontal distance in figure 5. Time histories of the measured force coefficients and Mach number are presented in figures 6 and 7. (Note that the scales of these figures change at 10 seconds.) Basic data cross plots of forces and moments for the two cylinders are shown in figure 8 for the fineness-ratio-2.56 cylinder and in figure 9 for the fineness-ratio-4.0 cylinder. The variation of the average center of pressure with Mach number is given in figure 10. An indication of the drag of the two cylinders is given in figure 11 where the longitudinal-force coefficient measured at low values of resultant force, $\sqrt{C_N^2 + C_Y^2}$, on the cylinders is plotted against Mach number.

DISCUSSION OF RESULTS

Time History

Fineness-ratio-2.56 cylinder.- A time history of C_N, C_Y, M, and C_R for the fineness-ratio-2.56 cylinder is shown in figure 6. The large disturbance at separation mentioned in the section called "Flight Tests" caused the instruments to exceed their calibrated ranges at each oscillation peak for about 1.5 seconds after cylinder-booster separation. During this time the cylinder decelerated from a Mach number of 1.7

to a Mach number of 0.9. The amplitude of the oscillation following the separating disturbance gradually decreased until the cylinder reached low subsonic speeds where an oscillation of low amplitude persisted for the remainder of the flight.

Fineness-ratio-4.0 cylinder with flared afterbody.- For the fineness-ratio-4.0 cylinder with flared afterbody, a time history of C_N, C_Y, M, and C_R is shown in figure 7. The times that the instruments exceeded their calibrated ranges is indicated on the time-history plot. A large-amplitude oscillation in pitch at separation damped until the cylinder reached low subsonic speeds where a low-amplitude oscillation similar to that of the fineness-ratio-2.56 cylinder persisted for the remainder of the flight. The disturbance in yaw caused by the firing of a pulse rocket at 5.6 seconds also damped until the cylinder reached low subsonic speeds. The resultant of the pitching and yawing motion C_R also shows damping following the two disturbances and displays the low-amplitude oscillation at low subsonic speeds which continues throughout the flight.

Basic Data Cross Plots

Fineness-ratio-2.56 cylinder.- Plots of C_N against C_Y presented in figure 8 for various Mach numbers show the model motion about trim which was discussed in detail in reference 3. The indication of rolling motion given by the angular displacement of adjacent peaks agrees closely with check values (not presented herein) obtained from the telemeter signal strength data. For the fineness-ratio-2.56 cylinder, this value is about 1 revolution per second. This rolling motion was probably caused by the roll of the cylinder-booster combination due to some small asymmetry in the booster.

Moment coefficients as a function of force coefficients for the yawing and pitching motions are shown in figure 8 for various Mach numbers. The moment curves are very nonlinear; the region of most stable slope is indicated to be near the zero force coefficient.

Fineness-ratio-4.0 cylinder with flared afterbody.- From the variation of C_N with C_Y (fig. 9) for various Mach numbers, it can be seen that a very low roll rate was present for the fineness-ratio-4.0 cylinder. This value is in agreement with check values obtained from the telemeter signal strength data; a roll rate of less than 1/2 revolution per second was indicated.

Some nonlinearity of the moment curves can be seen in the plots of figure 9 for various Mach numbers, the region of most stable slope being near the zero force coefficient.

Center of Pressure

The variation of the average center-of-pressure position with Mach number for the two cylinders of this test is presented in figure 10. The quality of the data precluded measurement of moment curve slopes at a particular force coefficient; therefore, a force-coefficient range of ±0.5 was selected and average slopes were read. Where the data permitted, average slopes were also read over a force-coefficient range of ±0.1 to show the region of most stable slope; the region was near the zero force coefficient. This type of nonlinearity has also been observed in data from the bluff shapes of references 4 and 5.

Over the force-coefficient range of ±0.5 for both cylinders of this test, the average center-of-pressure position moved toward the base as the speed decreased to subsonic Mach numbers. A qualitative comparison with right circular cylinders with fineness-ratio of 2.0 and 5.0 is furnished by the faired curves of data presented in reference 4. (See fig. 10.)

Drag

The drag level of the two cylinders is indicated in figure 11 by the variation of longitudinal-force coefficient measured at low values (C_N and C_Y usually less than 0.1) of the resultant-force coefficient with Mach number.

Comparison of the data from the present test for the fineness-ratio-2.56 cylinder, the data from reference 6 for the fineness-ratio-5.0 cylinder, and the data from the unpublished helium-gun free-flight tests for the fineness-ratio-12 cylinder indicates that the friction drag is a very small part of the total drag since about the same drag level is shown for all three cylinders. (See fig. 11(a).)

Since the fineness-ratio effect is indicated to be small, the difference of about 20-percent higher drag level at low supersonic speeds for the fineness-ratio-4.0 cylinder with a flared afterbody over that for the fineness-ratio-5.0 cylinder of reference 6 (fig. 11(b)) is thought to be caused by the presence of the flare. A somewhat similar bluff shape having a flared afterbody (unpublished helium-gun tests) indicates about the same drag level as was obtained with the flared cylinder of the present tests.

[redacted]

CONCLUDING REMARKS

A fineness-ratio-2.56 cylinder and a fineness-ratio-4.0 cylinder with flared afterbody have been tested in rocket-boosted axial free flight over a Mach number range of 0.4 to 1.7 and a Reynolds number range of 1×10^6 to 8×10^6. When given a large disturbance at supersonic speeds, both cylinders damped from a large-amplitude coupled motion at supersonic speeds to a low-amplitude sustained oscillation at low subsonic speeds. The variation of moment coefficient with force coefficient was nonlinear, the region of greatest stable slope occurring at the zero force coefficient. Although large pitching and yawing motions were observed for both cylinders, there were no large deviations from a ballistic flight path. For both cylinders the average center-of-pressure over the force-coefficient range of ±0.5 moved rearward with decrease in speed until the cylinder reached subsonic Mach numbers. Comparison of the drag data of this test with wind-tunnel and free-flight helium-gun data indicates that the friction drag is a very small part of the total drag. The presence of the afterbody flare on the fineness-ratio-4.0 cylinder causes an increase of about 20 percent of the total drag over the drag of a cylinder with no flare at low supersonic speeds.

Langley Aeronautical Laboratory,
National Advisory Committee for Aeronautics,
Langley Field, Va., December 5, 1956.

[redacted]

REFERENCES

1. Walchner, Otto, Weigand, Heinrich, and Kroeger, Hermann: Dynamic Stabilizer for the Finless Bluff Bomb. Tech. Note WCRR 54-53, Wright Air Dev. Center, U. S. Air Force, Apr. 19, 1954.

2. Carter, Howard S., and Lee, John B.: Investigation of the Ejection Release of Several Dynamically Scaled Bluff Internal Stores at Mach Numbers of 0.8, 1.39, and 1.98. NACA RM L56H28, 1956.

3. Nelson, Robert L.: The Motions of Rolling Symmetrical Missiles Referred to a Body-Axis System. NACA TN 3737, 1956.

4. Potter, J. Leith, Murphree, William D., and Shapiro, Norman M.: Normal Force and Center of Pressure on Right Circular Cylinders. Jour. Aero. Sci. (Readers' Forum), vol. 22, no. 3, Mar. 1955, pp. 214-215.

5. Loeb, A. A.: Transonic Wind Tunnel Tests of 90 mm, T294, HEP Shell, Finned and Bluffshapes. Tech. Memo. No. 5., Samuel Feltman Ammunition Labs., Picatinny Arsenal (Dover, N. J.), Mar. 1, 1956.

6. Walchner, O.: Systematic Wind-Tunnel Measurements on Missiles. NACA TM 1122, 1947.

[redacted]

TABLE I

PHYSICAL CONSTANTS FOR CYLINDERS TESTED

	Fineness-ratio-2.56 cylinder	Fineness-ratio-4.0 cylinder with flared afterbody
W, lb	71.0	69.5
I_X, slug-ft^2	0.121	0.137
I_Y, slug-ft^2	0.575	0.891
I_Z, slug-ft^2	0.575	0.891
$\frac{x_{cg}}{l}$	0.323	0.250
d, ft	0.666	0.666
l, ft	1.708	2.667
S, ft^2	0.348	0.348

[redacted]

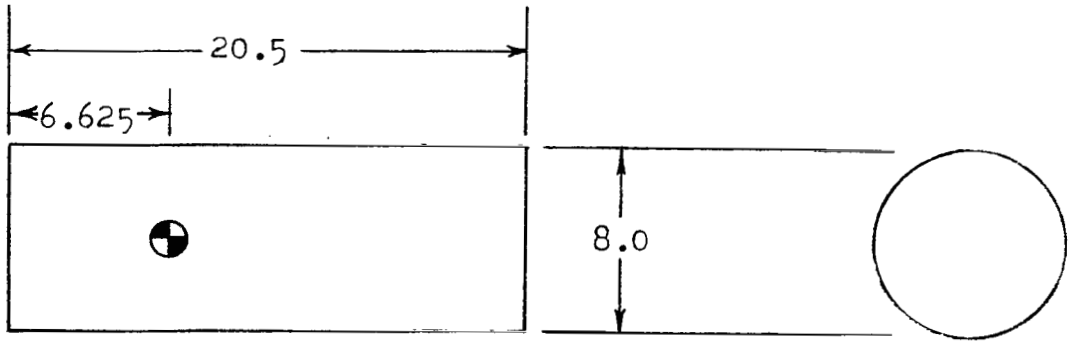

(a) Fineness-ratio-2.56 cylinder.

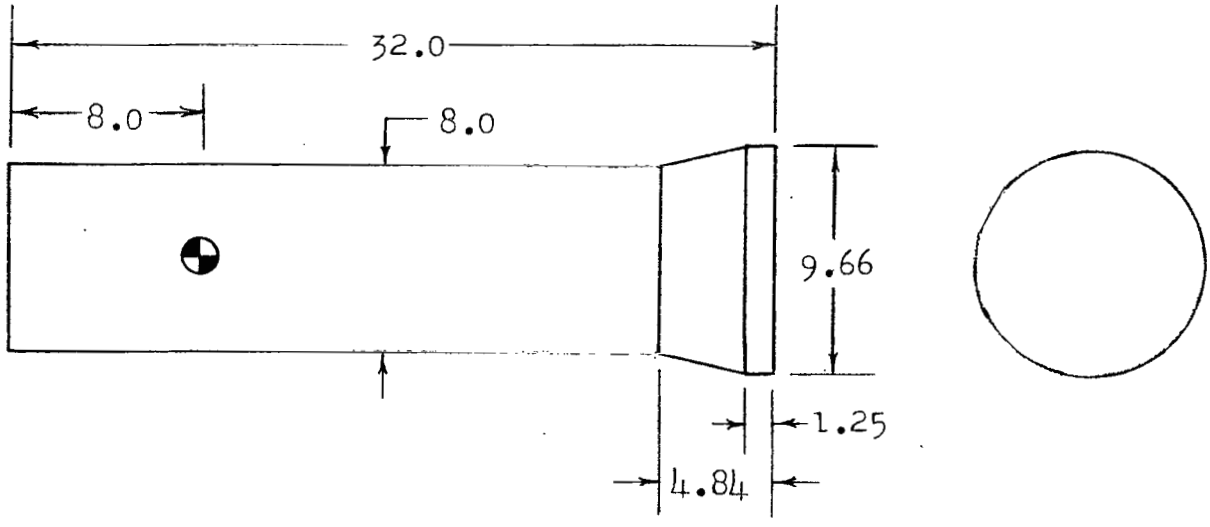

(b) Fineness-ratio-4.0 cylinder with flared afterbody.

Figure 1.- Drawings of cylinders tested. All dimensions are in inches.

(a) Fineness-ratio-2.56 cylinder. L-92839

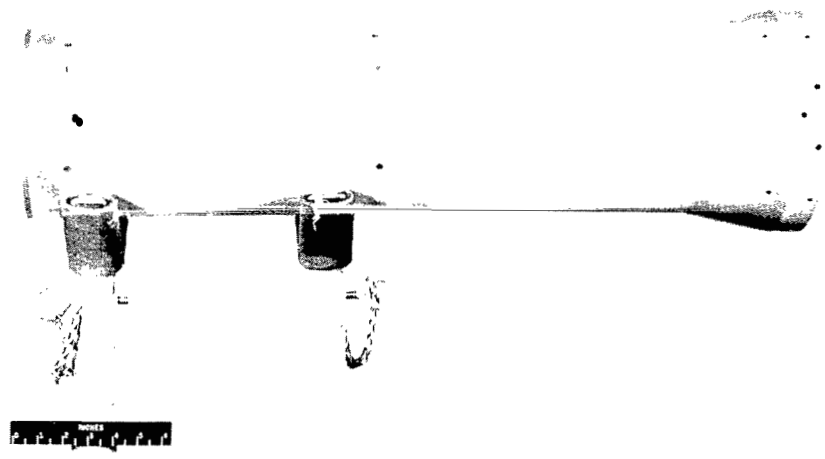

(b) Fineness-ratio-4.0 cylinder with flared afterbody. L-93633

Figure 2.- Photographs of cylinders tested.

[redacted]

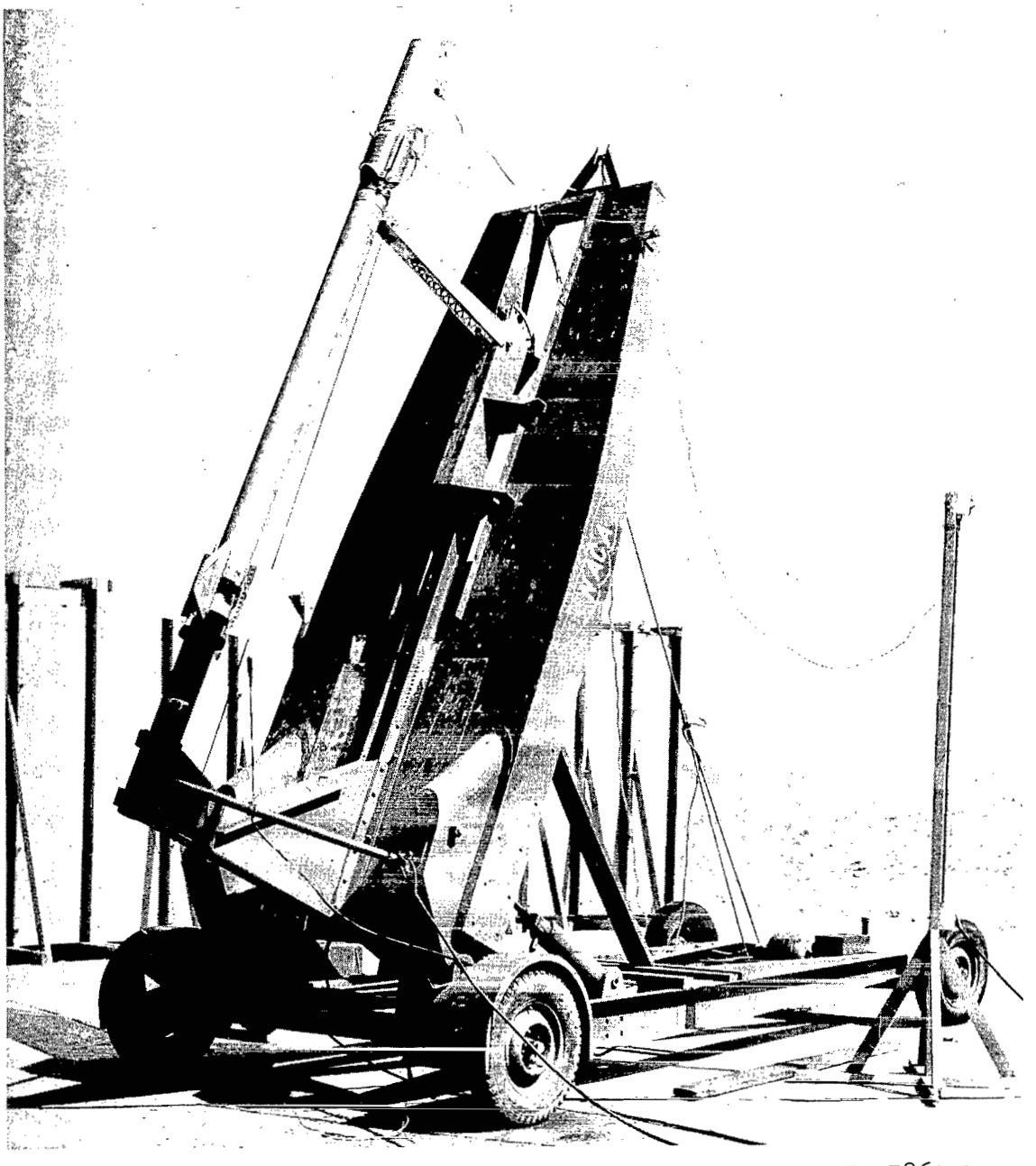

L-93862.1

(c) Fineness-ratio-2.56 cylinder on booster in launching position.

Figure 2.- Continued.

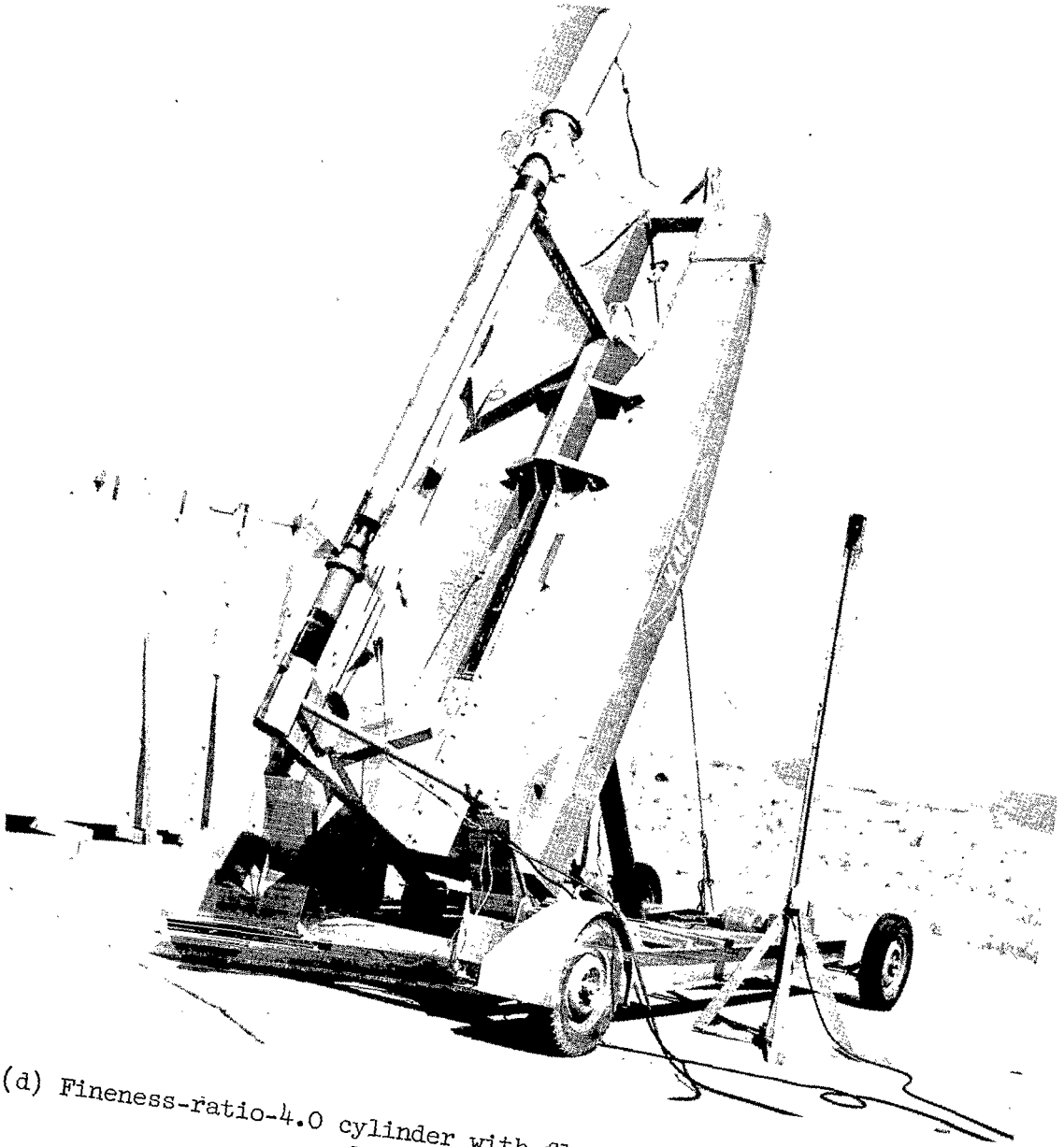

(d) Fineness-ratio-4.0 cylinder with flared afterbody on booster in launching position. L-93425.1

Figure 2.- Concluded.

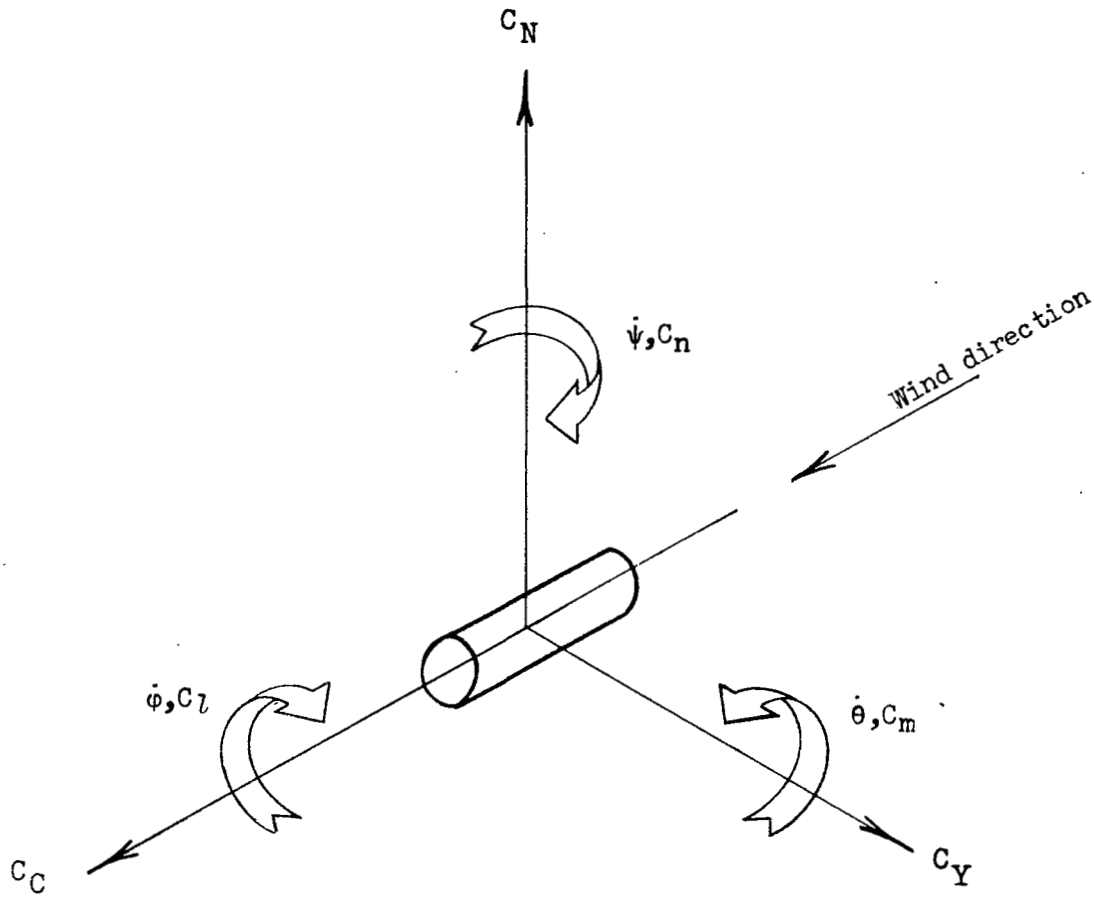

Figure 3.- Axes system showing positive directions of force and moment coefficients and angular velocities.

[redacted]

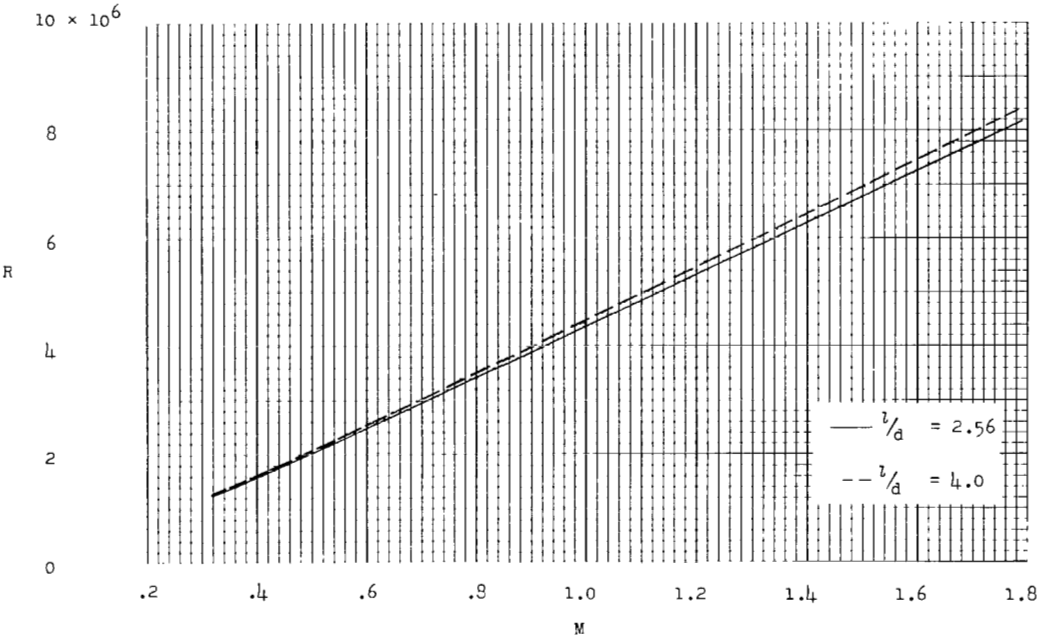

Figure 4.- Reynolds number of tests based on cylinder diameter.

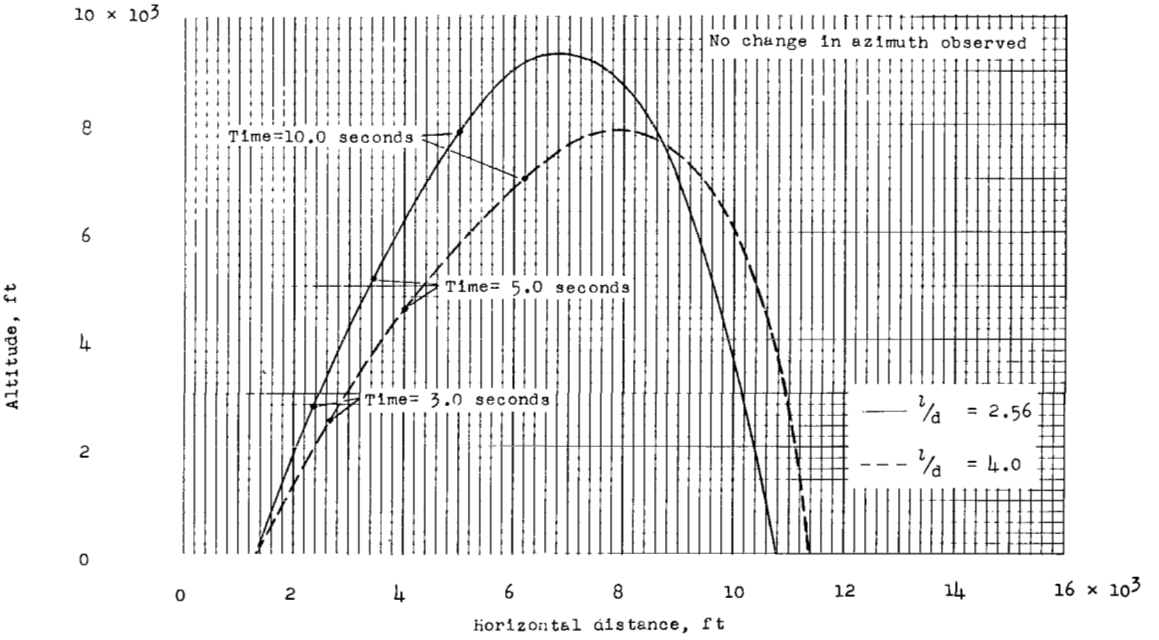

Figure 5.- Flight paths of cylinders tested.

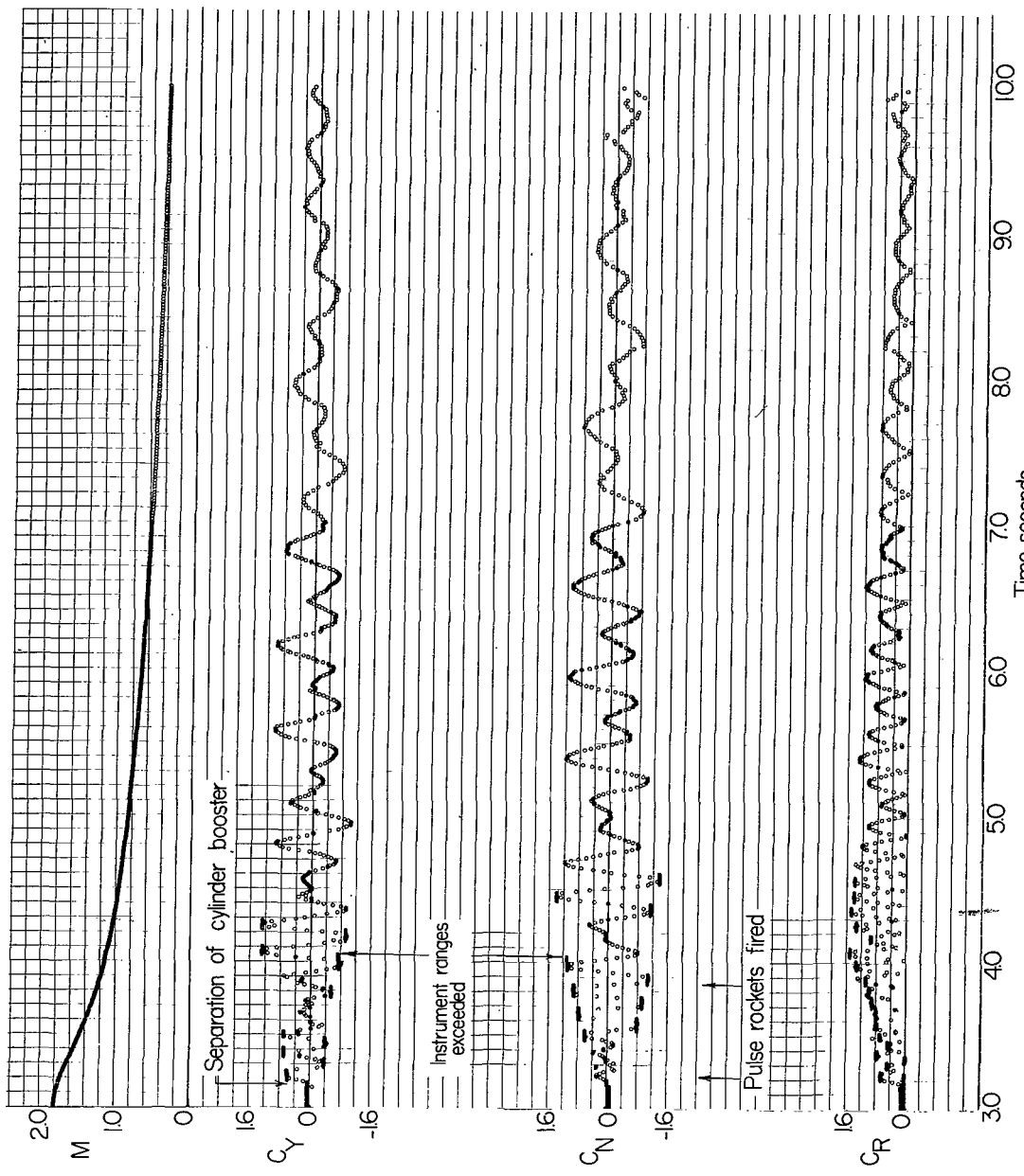

Figure 6.- Time history of fineness-ratio-2.56 cylinder. (Note that scales change at 10.0 seconds.

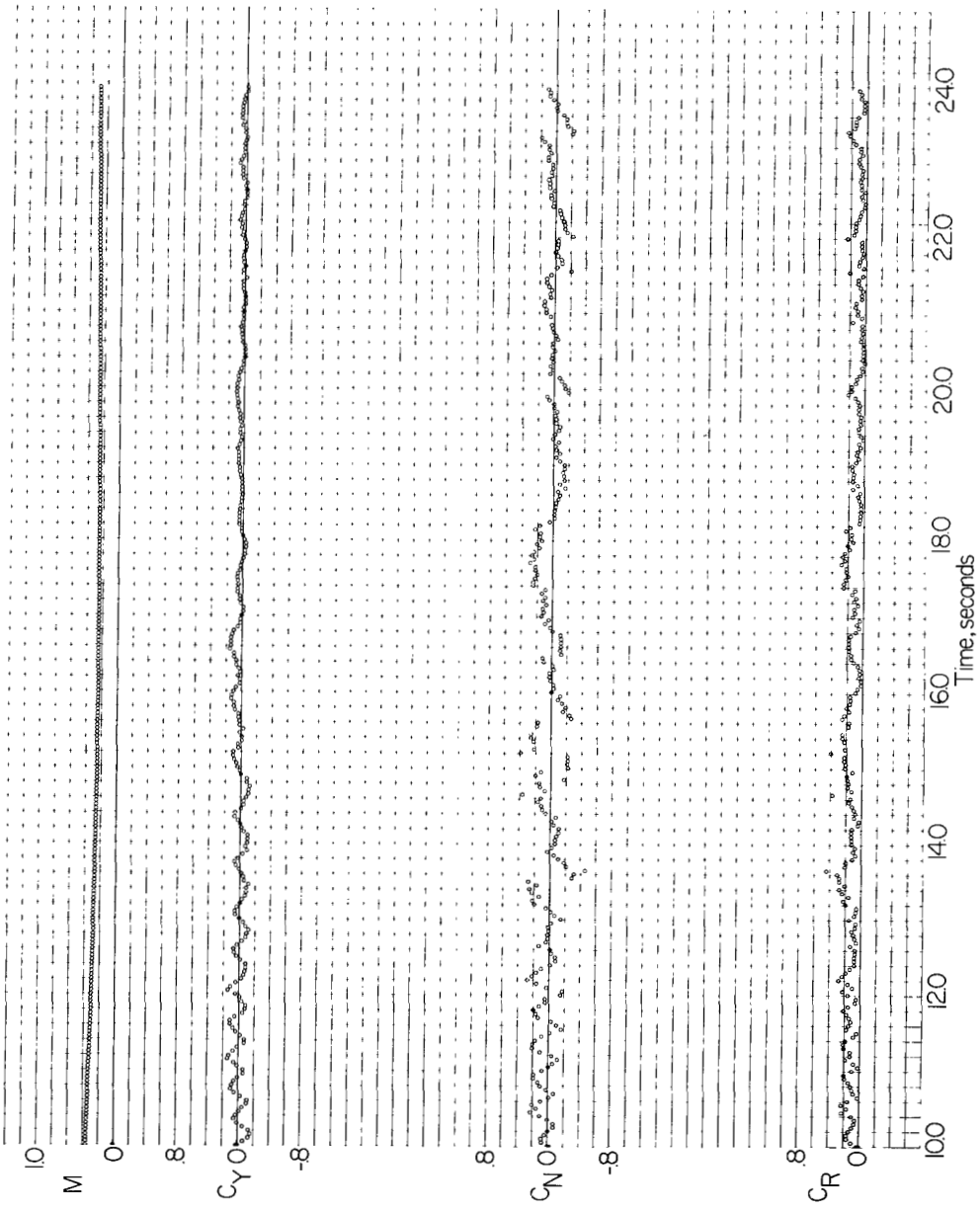

Figure 6.- Continued.

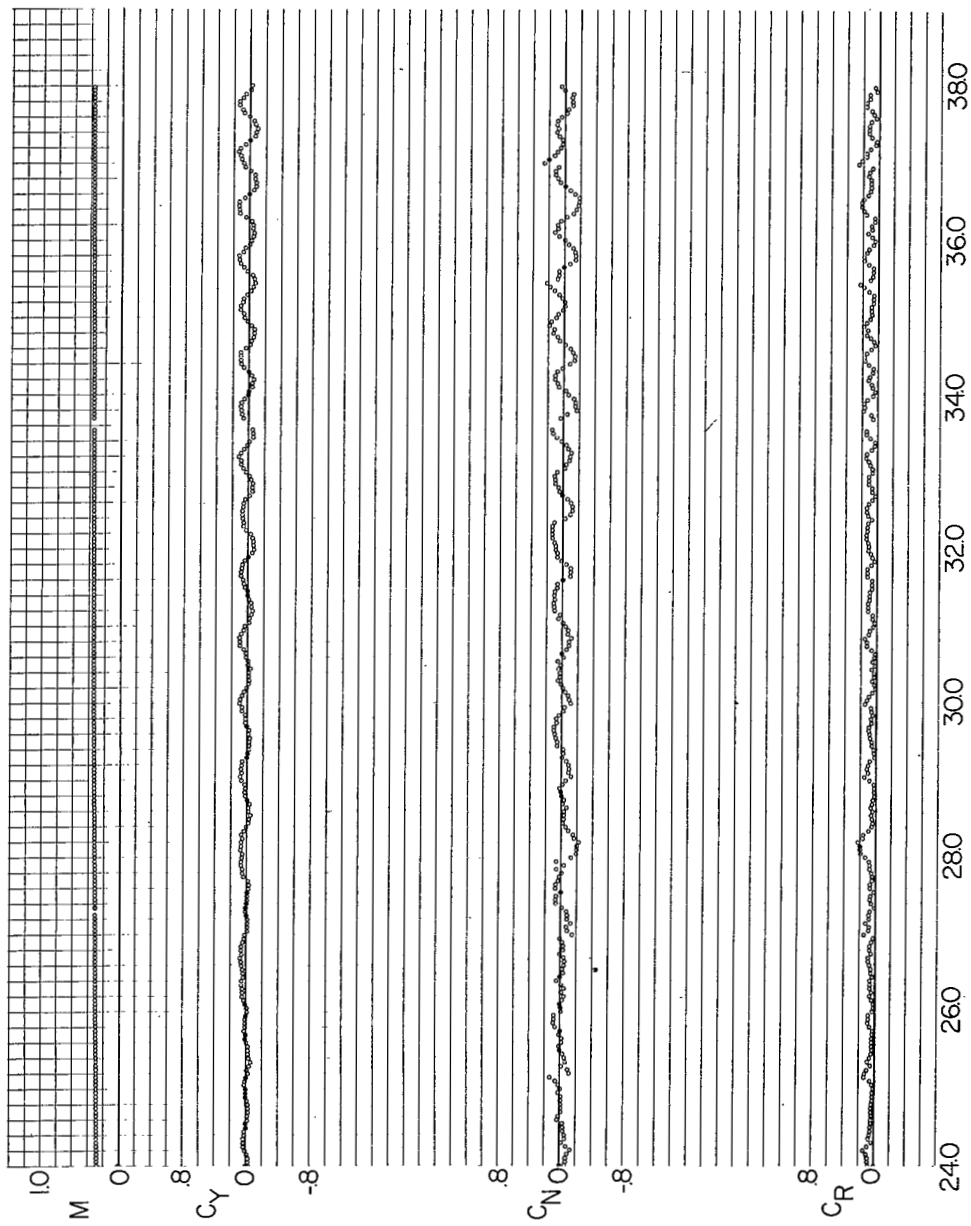

Figure 6.- Concluded.

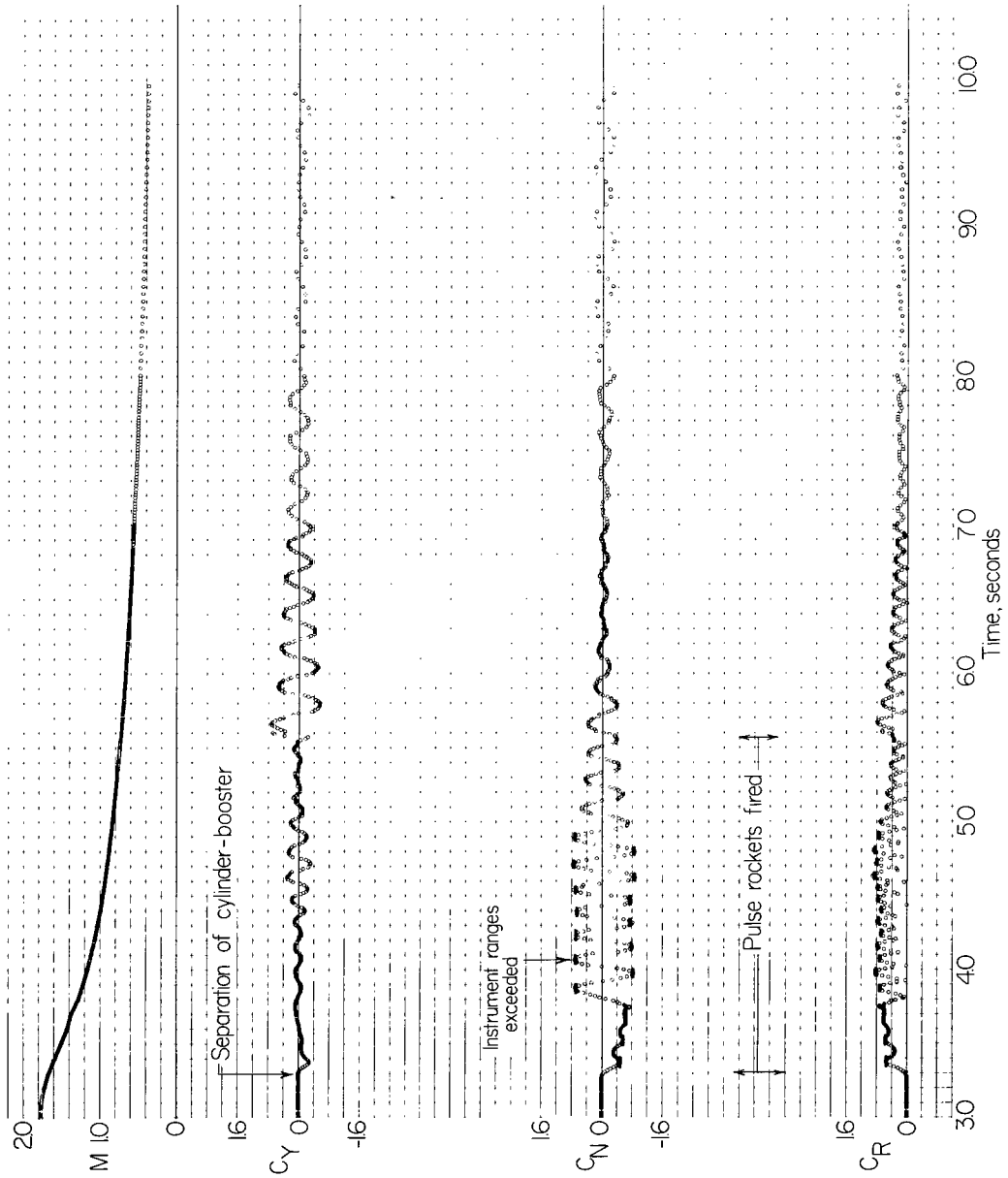

Figure 7.- Time history of fineness-ratio-4.0 cylinder with flared afterbody. (Note that scales change at 10.0 seconds.)

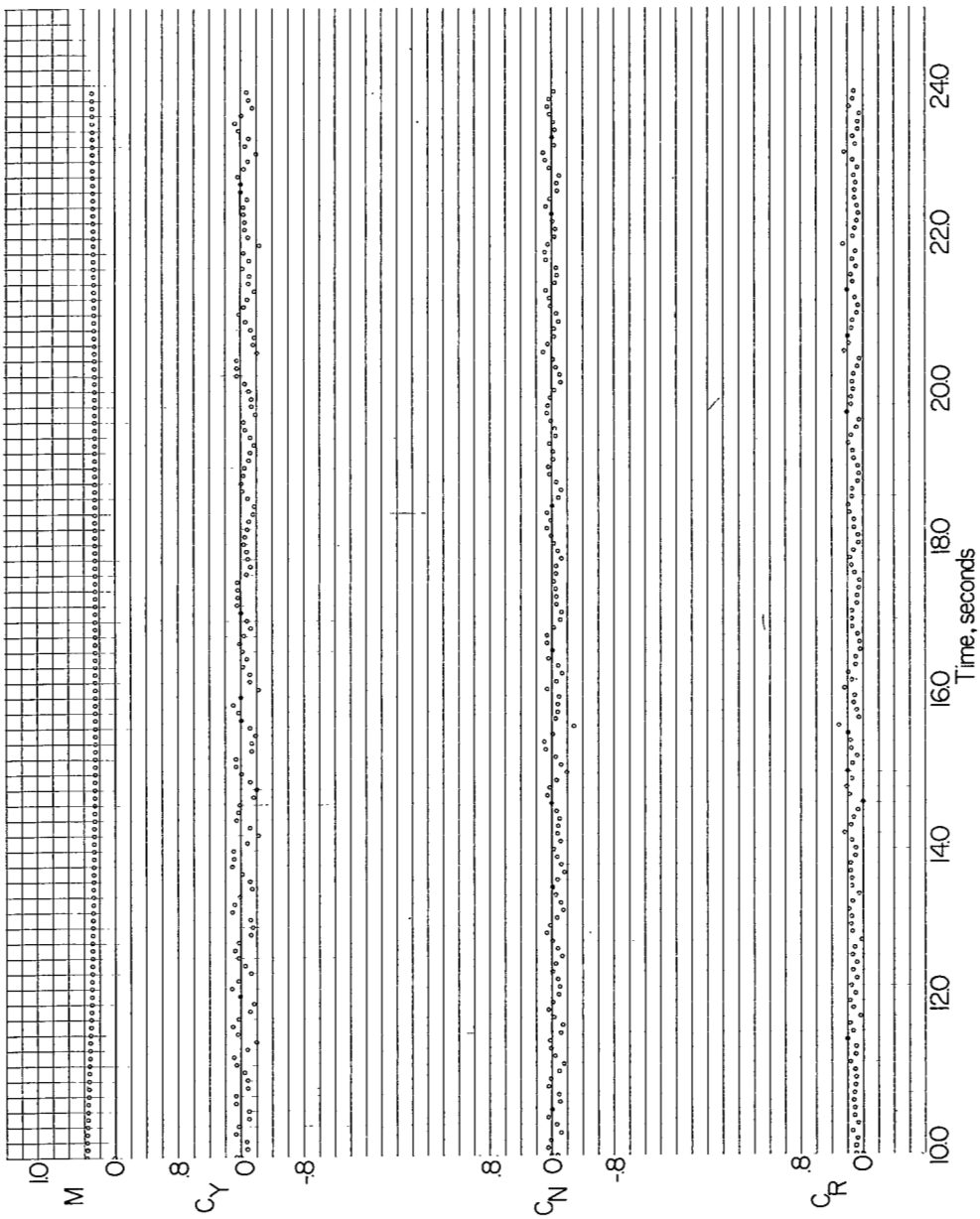

Figure 7.- Continued.

[redacted]

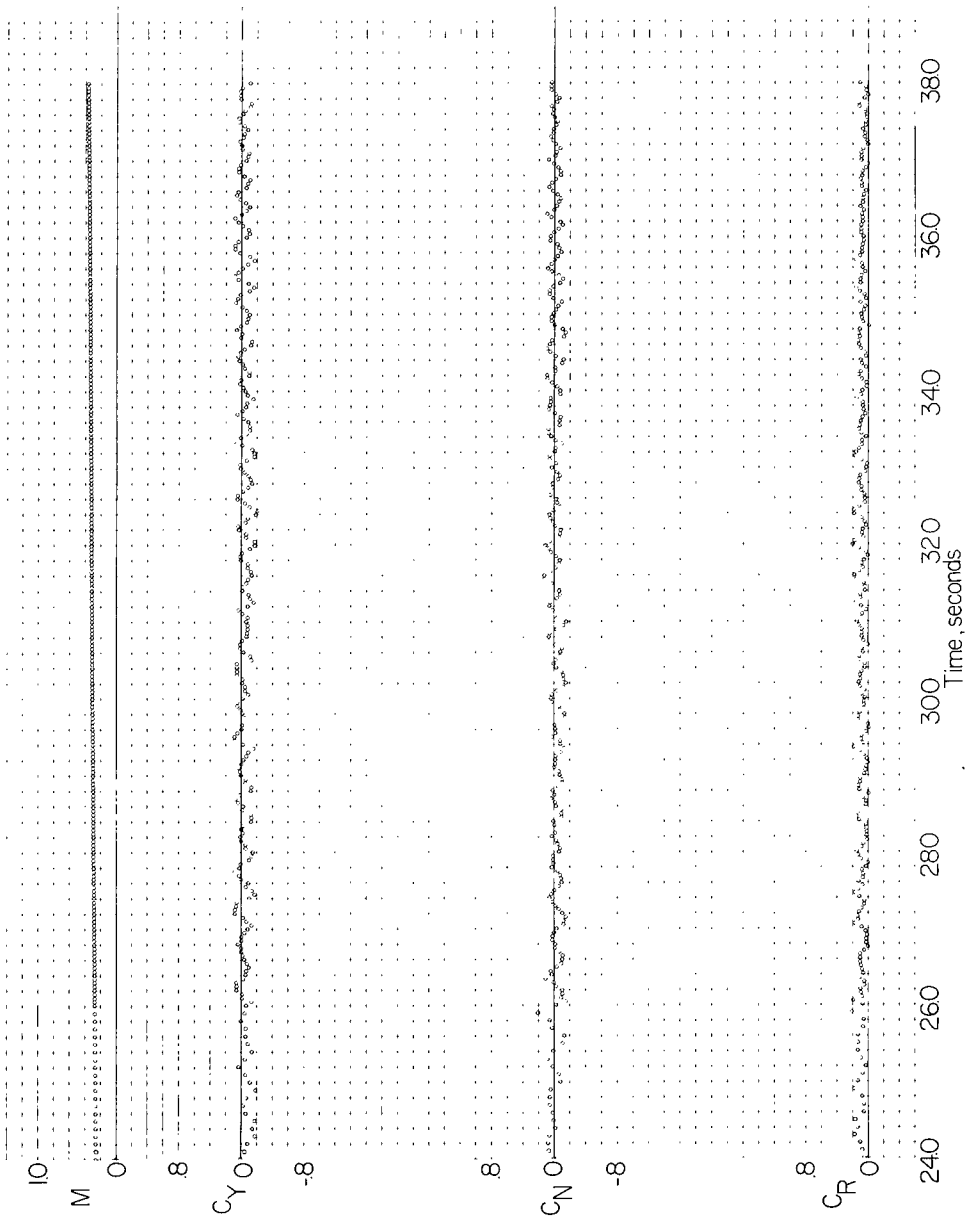

Figure 7.- Concluded.

[redacted]

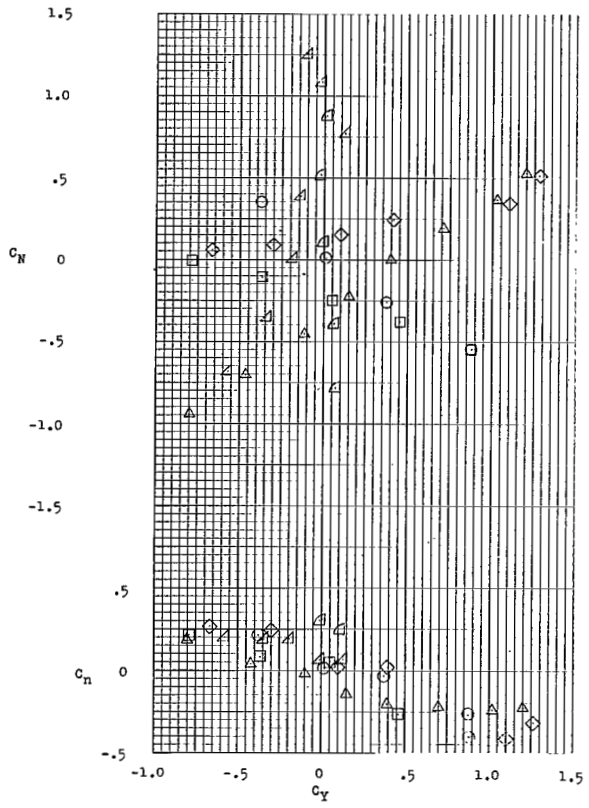

○,□,◇,△,⊿,◰ Time sequence of cross-plot symbols; symbol changes at each maximum and each minimum value of C_Y

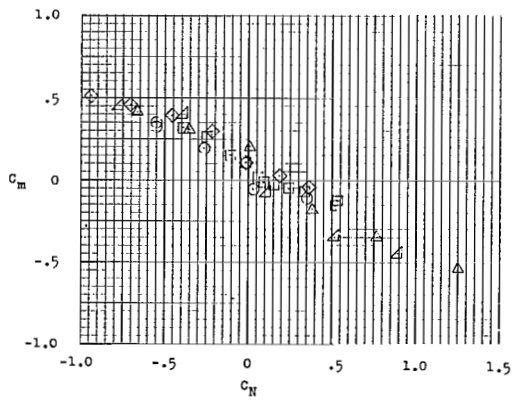

(a) M = 1.14 to M = 0.93.

Figure 8.- Basic data cross plots of force and moment coefficients for the fineness-ratio-2.56 cylinder.

[redacted]

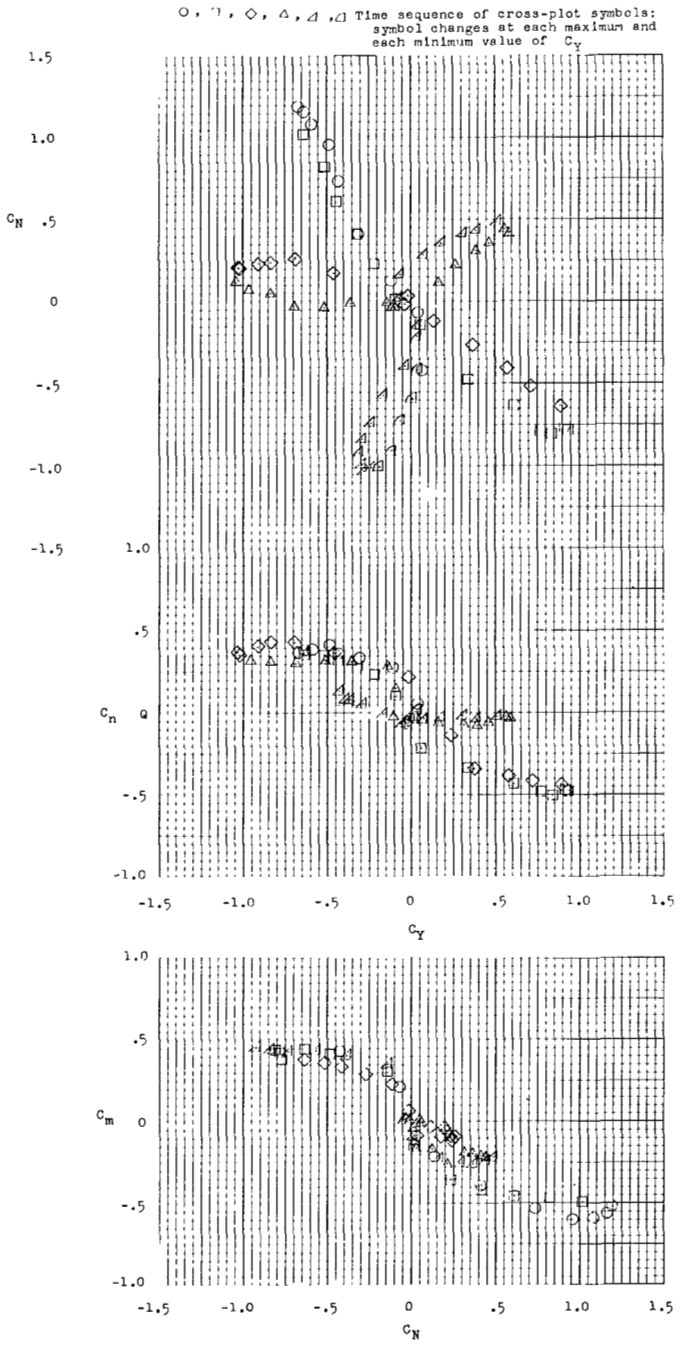

(b) M = 0.93 to M = 0.78.

Figure 8.- Continued.

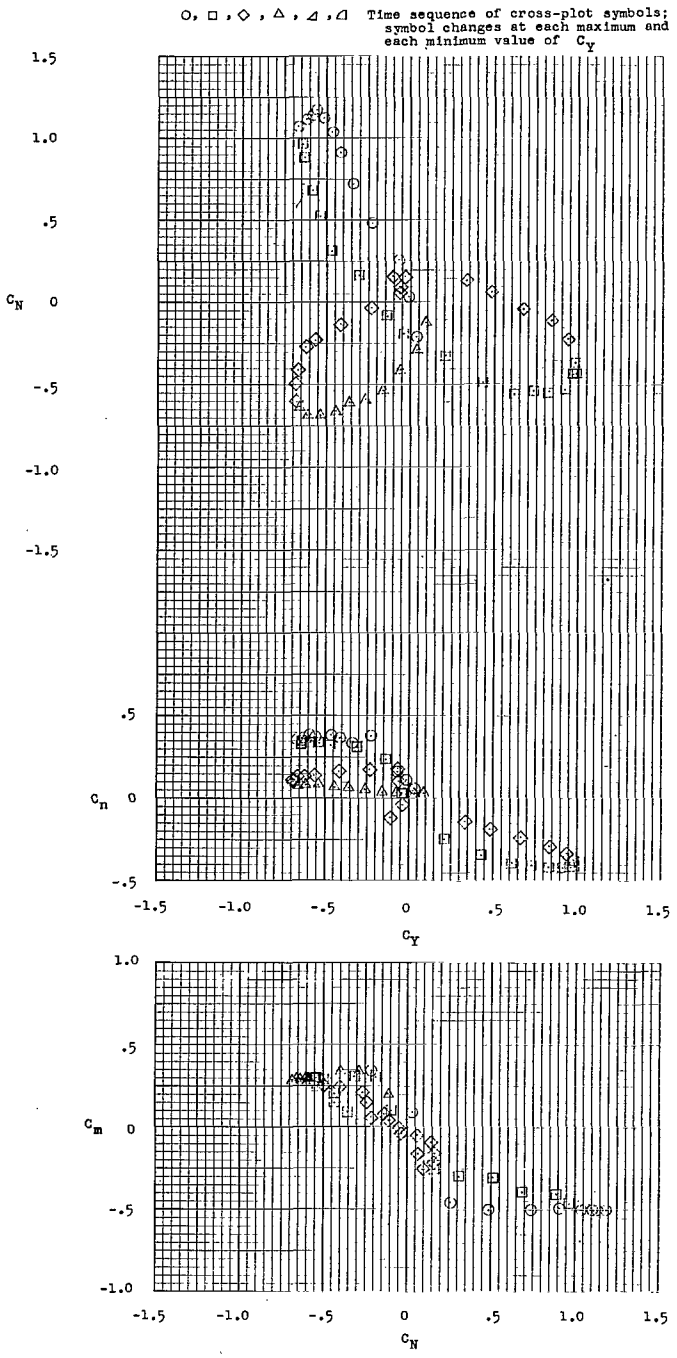

(c) M = 0.78 to M = 0.69.

Figure 8.- Continued.

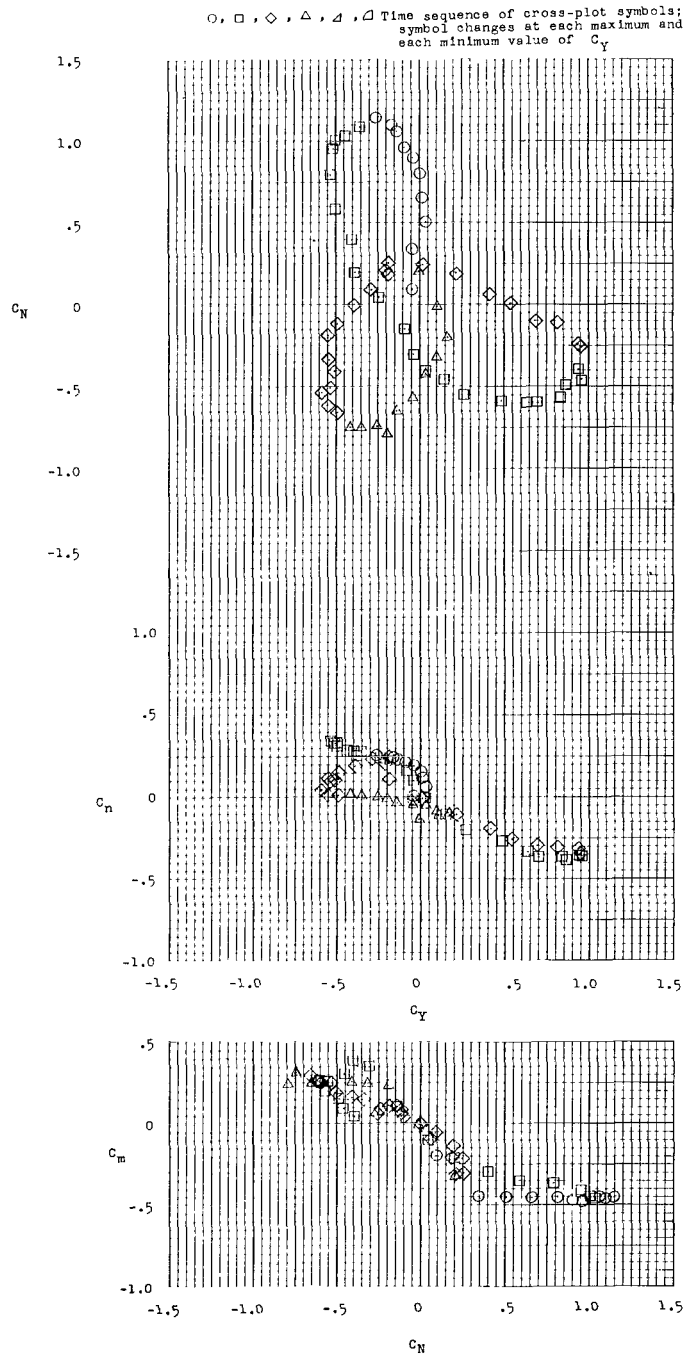

(d) M = 0.69 to M = 0.61.

Figure 8.- Continued.

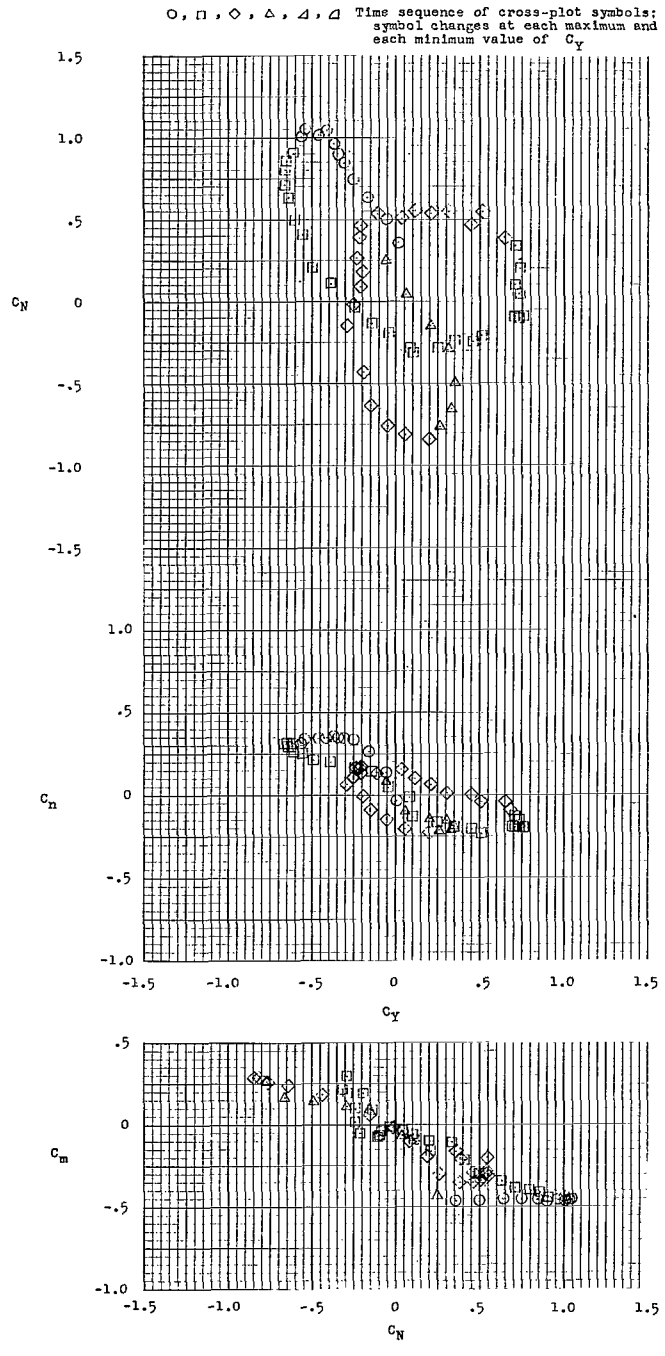

(e) M = 0.61 to M = 0.54.

Figure 8.- Continued.

[redacted]

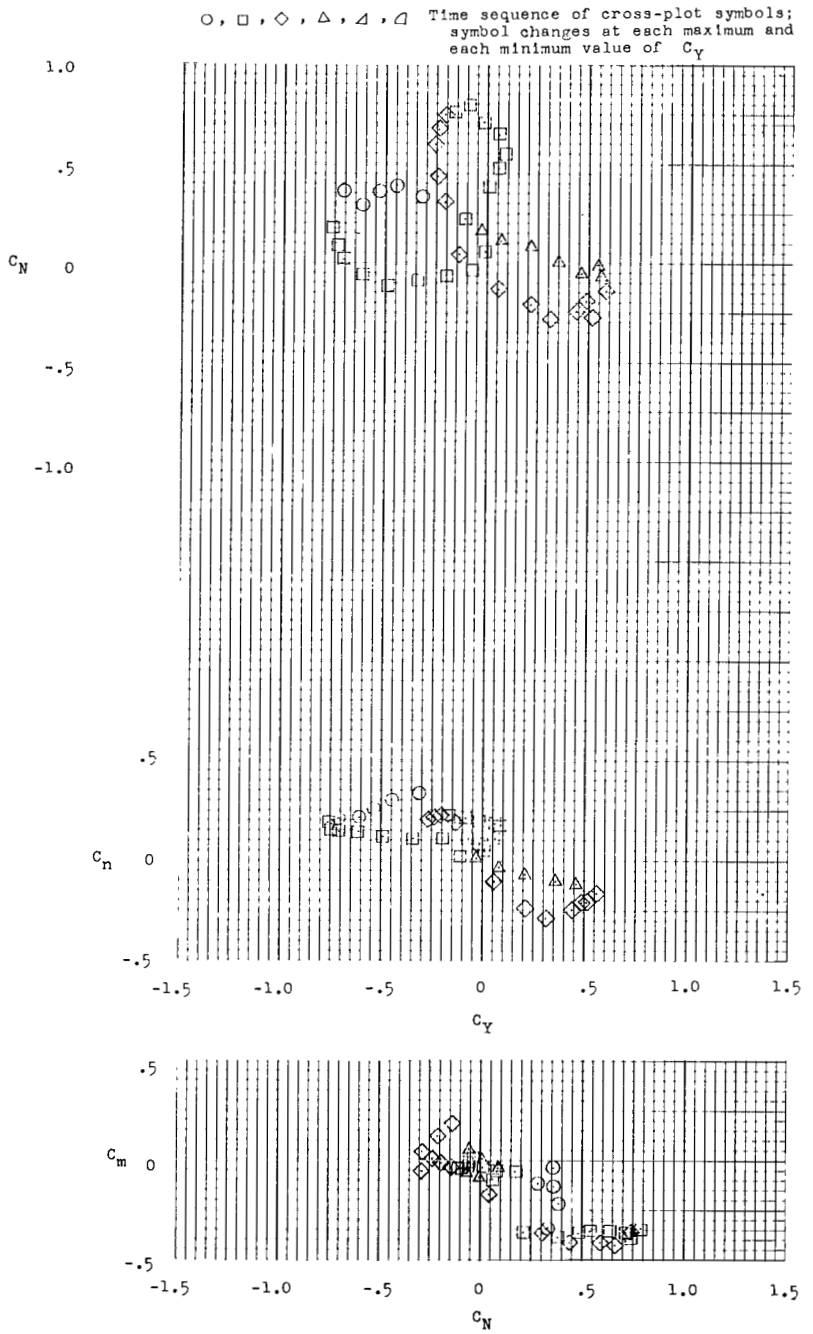

(f) M = 0.54 to M = 0.47.

Figure 8.- Continued.

[redacted]

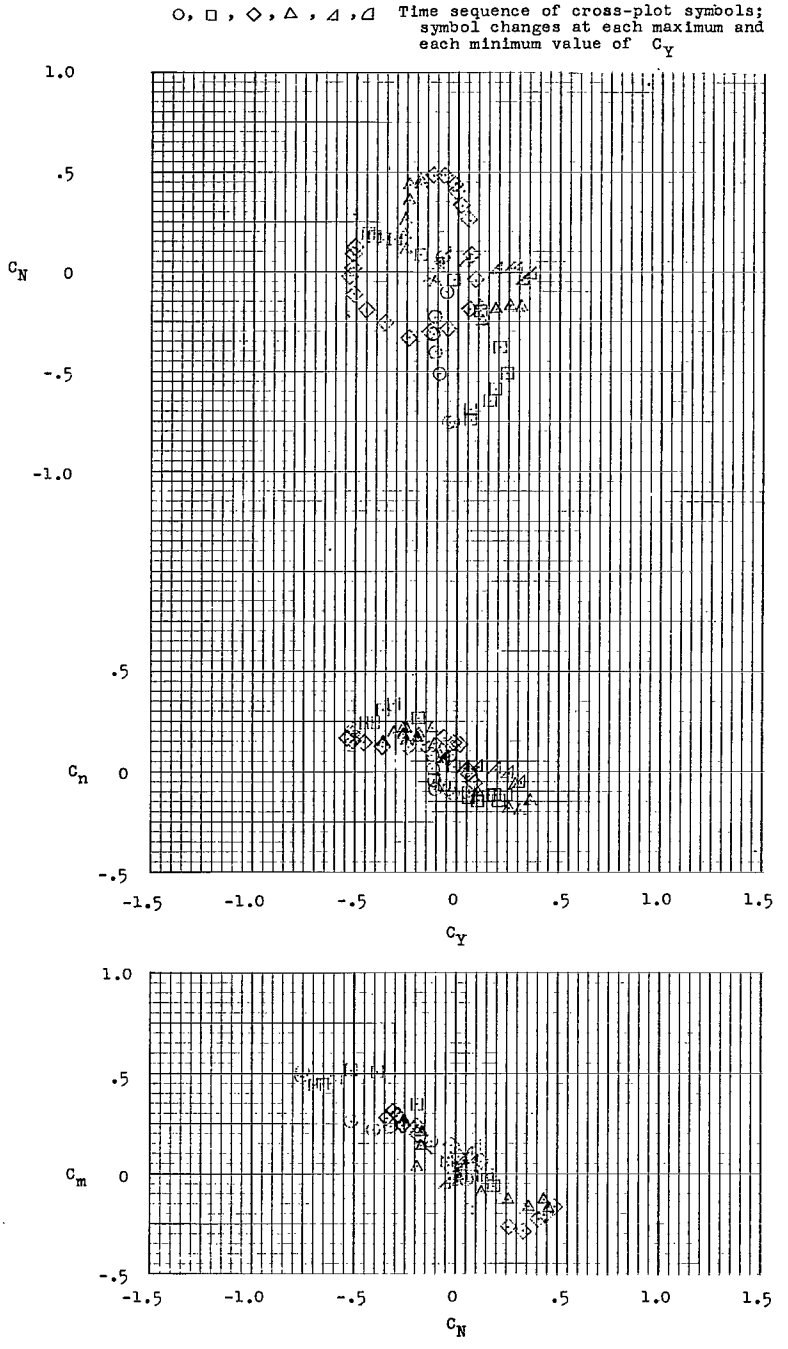

(g) M = 0.47 to M = 0.39.

Figure 8.- Concluded.

[redacted]

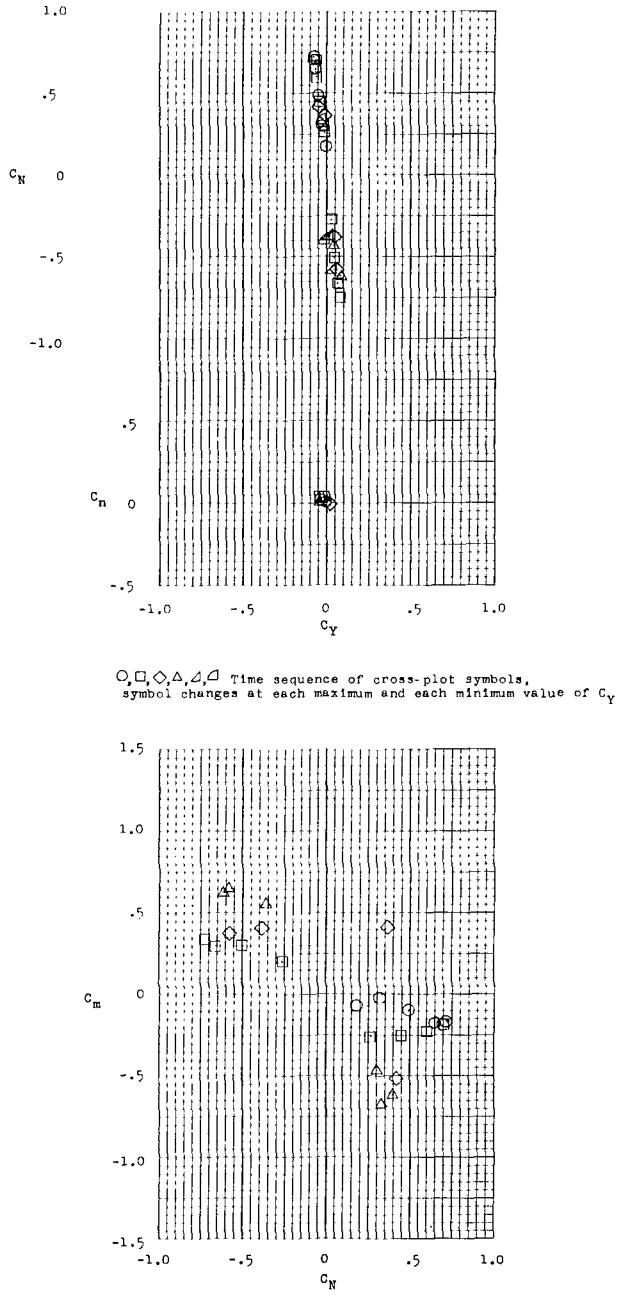

(a) M = 1.28 to M = 1.03.

Figure 9.- Basic data cross plots of force and moment coefficients for fineness-ratio-4.0 cylinder with flared afterbody.

[redacted]

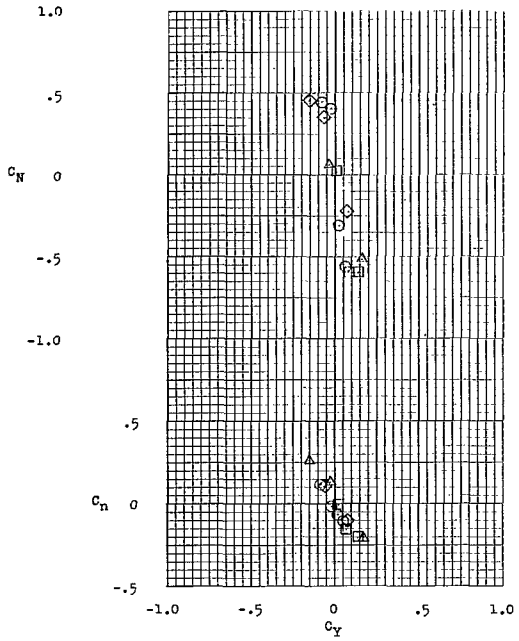

○, □, ◇, △, ◿, ◿ Time sequence of cross-plot symbols; symbol changes at each maximum and each minimum value of C_Y

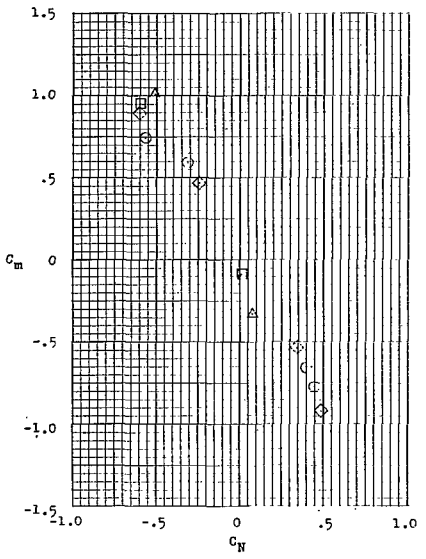

(b) M = 1.03 to M = 0.85.

Figure 9.- Continued.

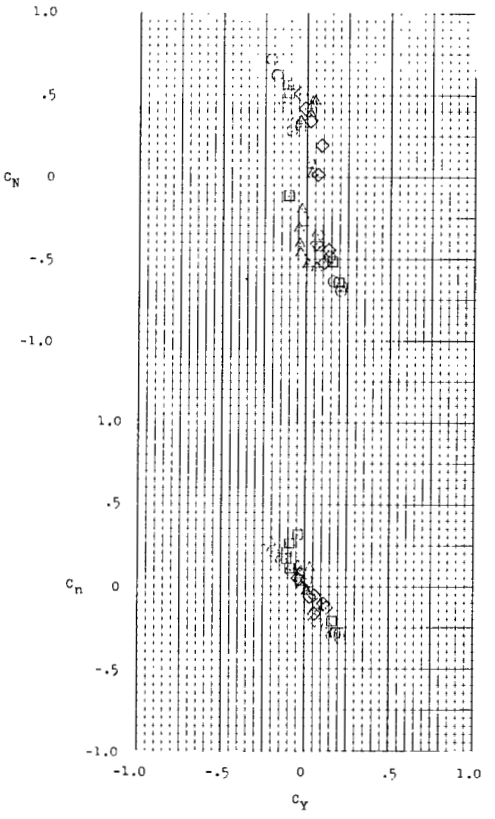

○, □, ◇, △, ▽, ◁ Time sequence of cross-plot symbols; symbol changes at each maximum and each minimum value of C_Y

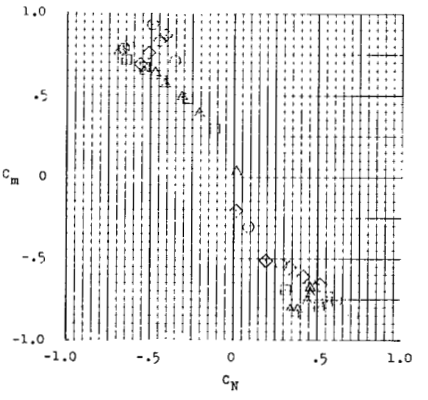

(c) M = 0.85 to M = 0.77.

Figure 9.- Continued.

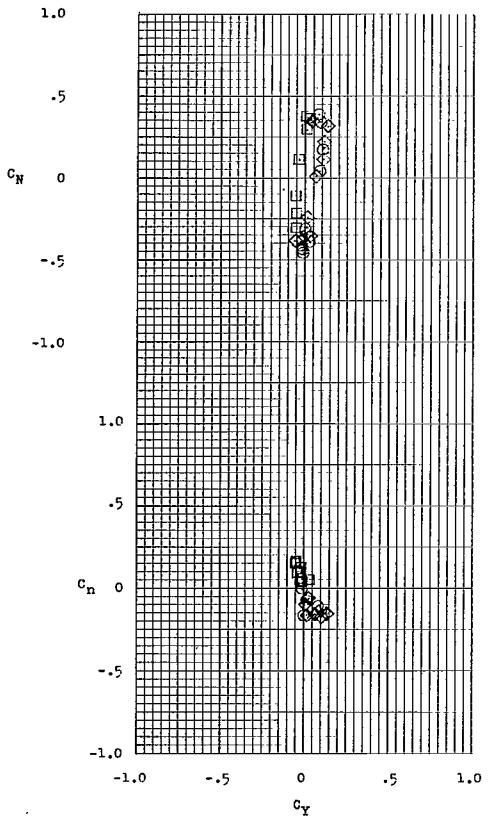

○, □, ◇, △, ⊿, ⊿ Time sequence of cross-plot symbols; symbol changes at each maximum and each minimum value of C_Y

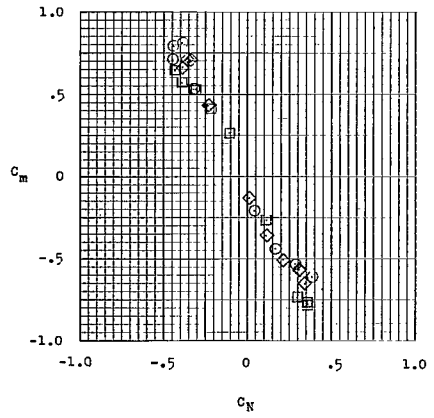

(d) M = 0.77 to M = 0.73.

Figure 9.- Continued.

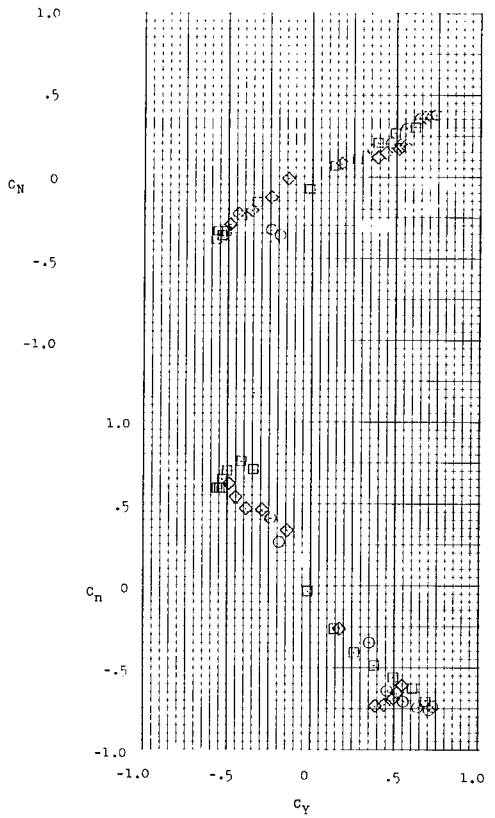

○, □, ◇, △, ⊿, ◿ Time sequence of cross-plot symbols; symbol changes at each maximum and each minimum value of C_Y

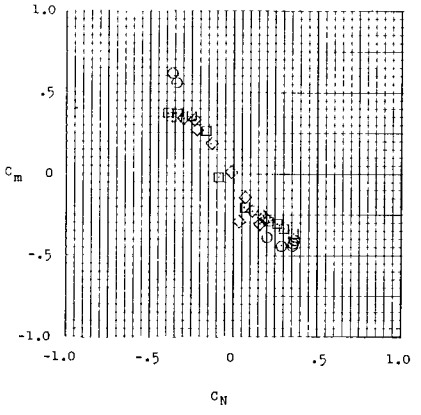

(e) M = 0.73 to M = 0.67.

Figure 9.- Continued.

[redacted]

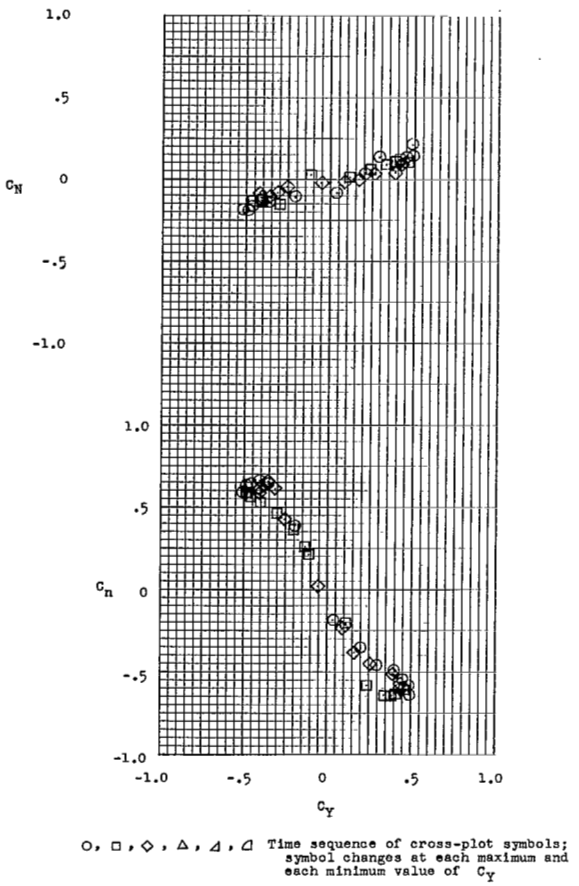

(f) M = 0.67 to M = 0.62.

Figure 9.- Continued.

[redacted]

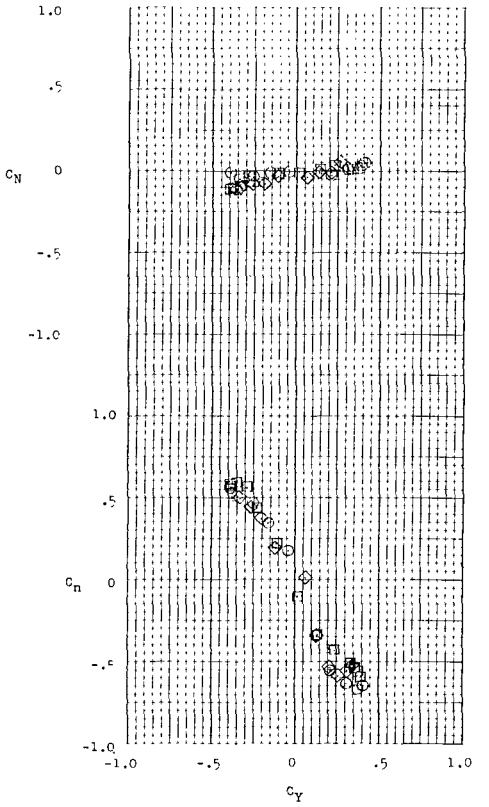

O, □, ◇, △, ◁, ◻ Time sequence of cross-plot symbols; symbol changes at each maximum and each minimum value of C_Y

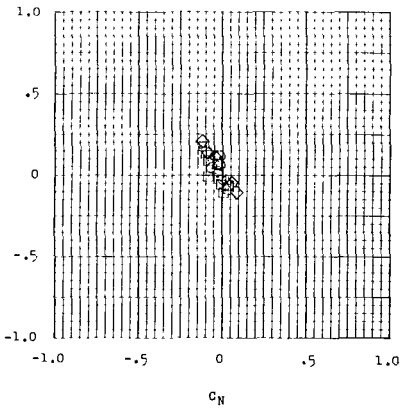

(g) M = 0.62 to M = 0.58.

Figure 9.- Continued.

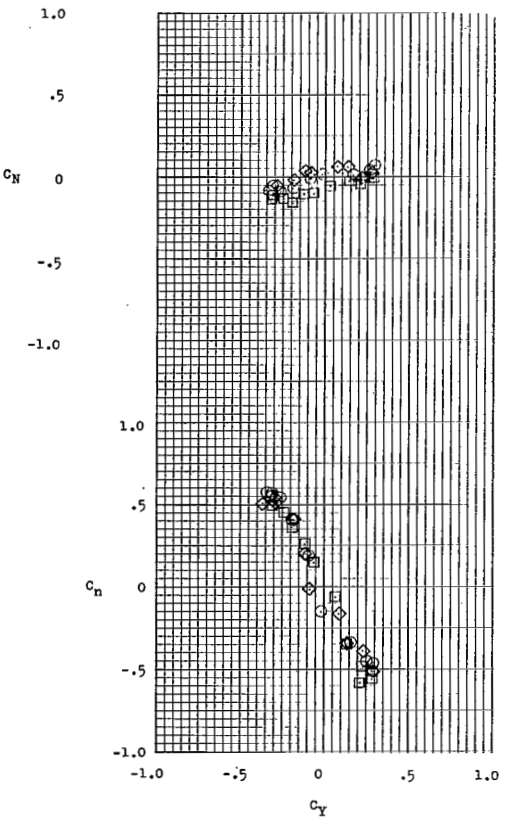

○, ▣, ◇, △, ◿, ◺ Time sequence of cross-plot symbols; symbol changes at each maximum and each minimum value of C_Y

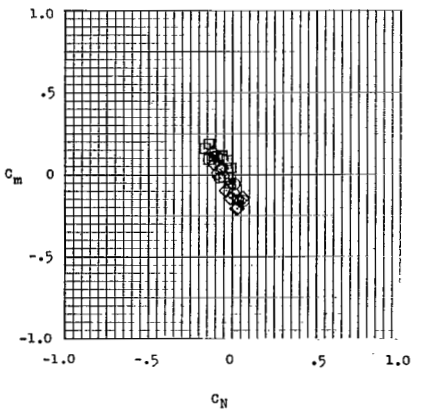

(h) M = 0.58 to M = 0.56.

Figure 9.- Continued.

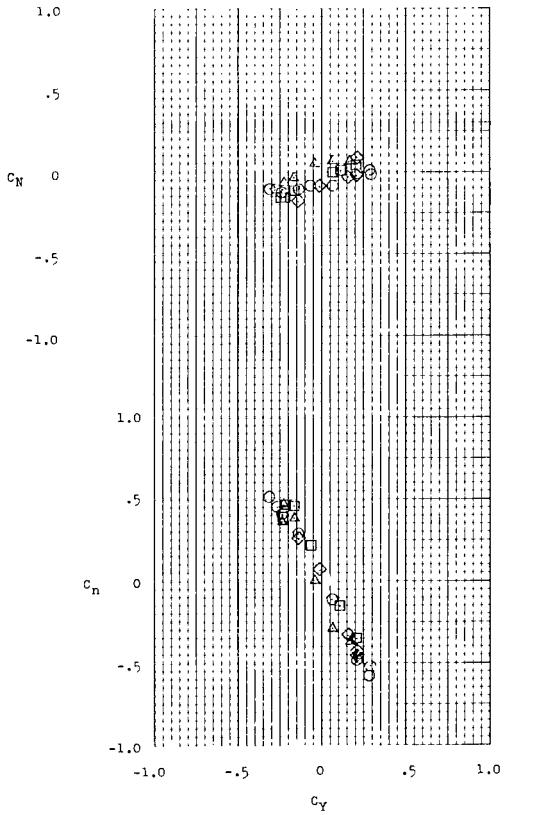

(i) M = 0.56 to M = 0.52.

Figure 9.- Continued.

[redacted]

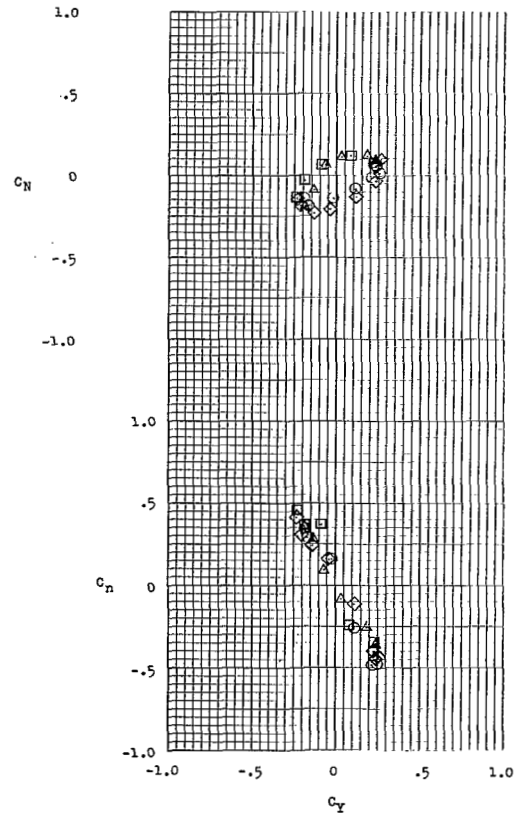

○, □, ◇, △, ◿, ◿ Time sequence of cross-plot symbols; symbol changes at each maximum and each minimum value of C_Y

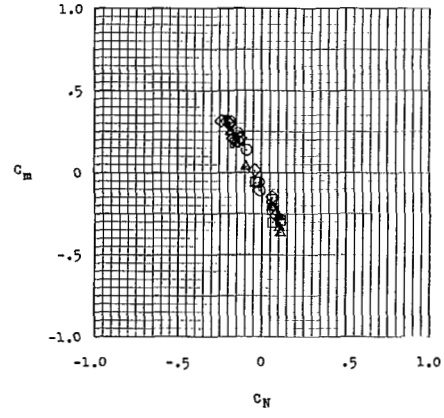

(j) M = 0.52 to M = 0.48.

Figure 9.- Continued.

[redacted]

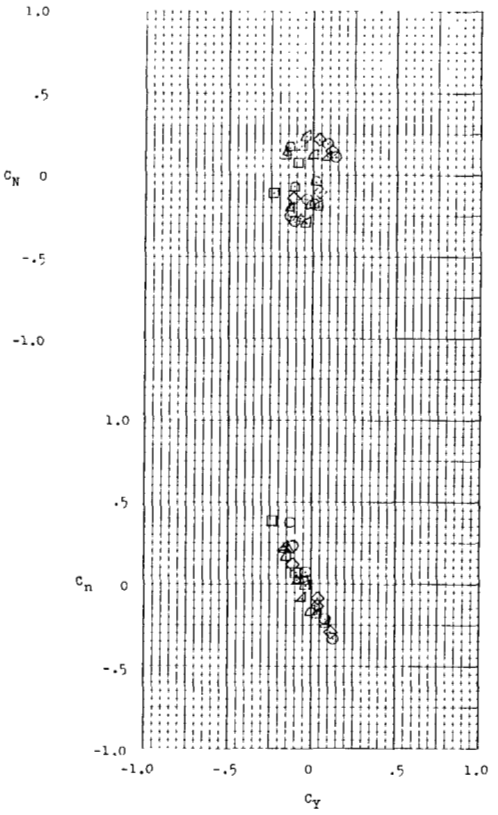

(k) M = 0.48 to M = 0.40.

Figure 9.- Concluded.

[redacted]

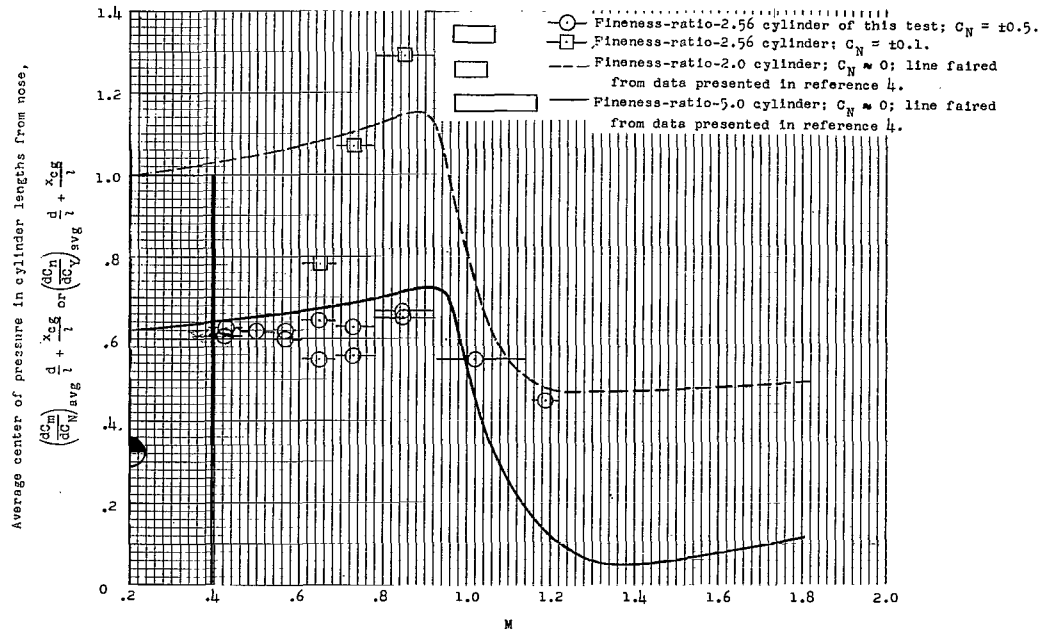

(a) Fineness-ratio-2.56 cylinder.

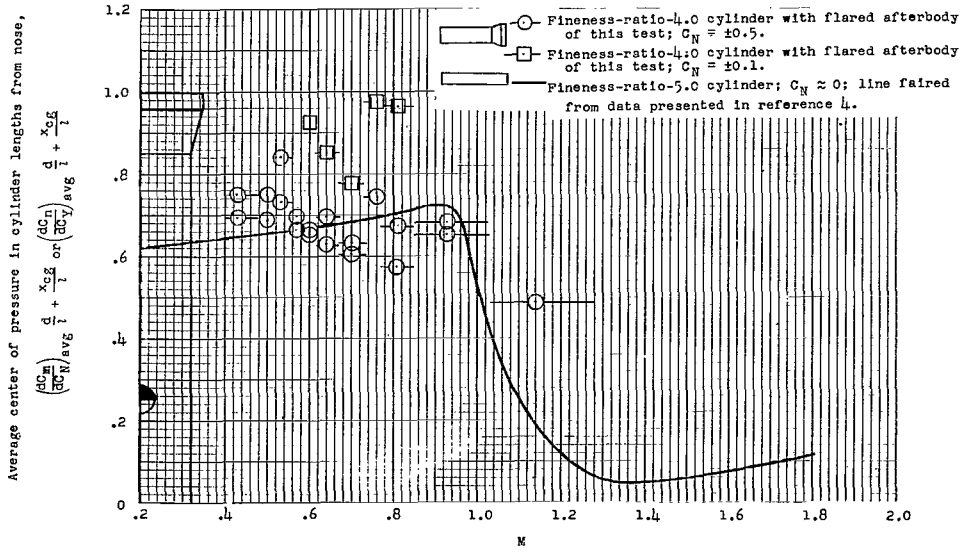

(b) Fineness-ratio-4.0 cylinder with flared afterbody.

Figure 10.- Variation of average center of pressure with Mach number. Line extensions on symbols indicate Mach number range used to obtain data point.

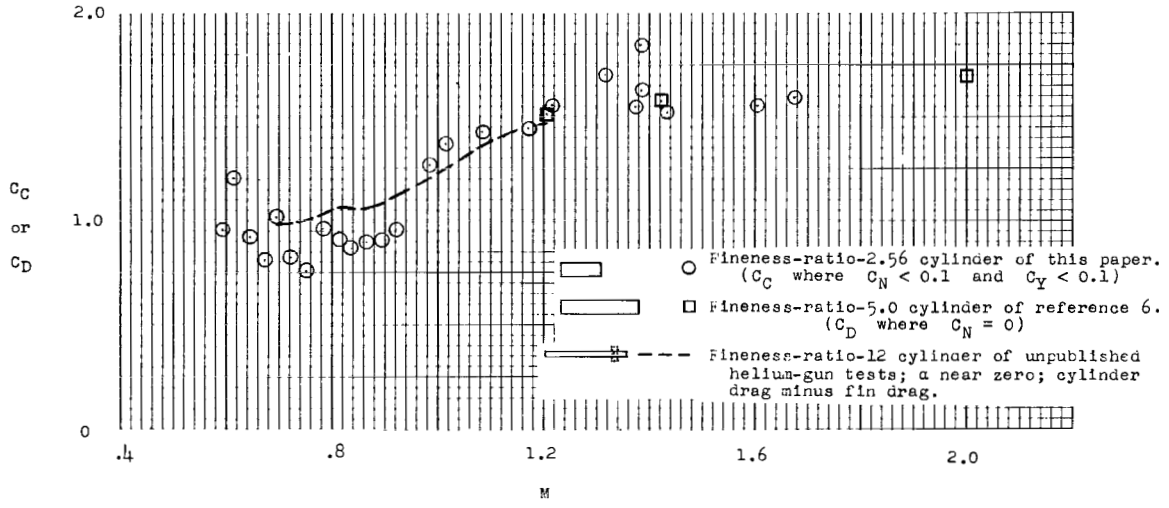

(a) Fineness-ratio-2.56 cylinder.

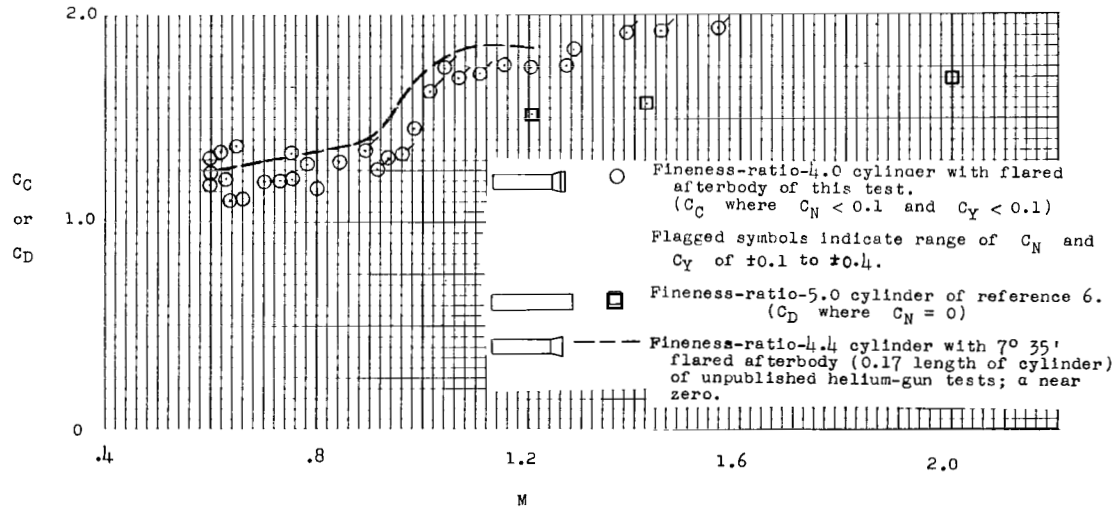

(b) Fineness-ratio-4.0 cylinder with flared afterbody.

Figure 11.- Variation of longitudinal-force coefficient with Mach number.